An Autonomous Driving model with BEV-V2X Perception, Trajectory Prediction and Driving Planning in Complex Traffic Intersections

Fukang Li*, Owen Lin, Kunpeng Gao, Yifei Li*

Ford Motor China Co.,ltd, Shanghai, 200082, China

Abstract

The comprehensiveness of vehicle-to-everything (V2X) recognition enriches and holistically shapes the global Birds-Eye-View (BEV) perception, incorporating rich semantics and integrating driving scene information, thereby serving features of trajectory prediction, decision-making and driving planning. Utilizing V2X message sets to form BEV format proves to be an effective perception method for connected and automated vehicles (CAVs). Specifically, MAP, SPAT and RSI data contributes to the achievement of road connectivity, synchronized traffic signal navigation and obstacle warning. Moreover, using time-sequential BSMs information from multiple vehicles allows for the perception of current state and the prediction of future trajectories. Therefore, this paper develops a comprehensive autonomous driving model that relies on BEV-V2X perception, Interacting Multiple model Unscented Kalman Filter (IMM-UKF)-based trajectory prediction, and deep reinforcement learning (DRL)-based decision making and planing. We establish a DRL environment with reward-shaping methods to formulate a unified set of optimal driving behaviors that encompass obstacle avoidance, lane changes, overtaking, turning maneuver, and synchronized traffic signal navigation. Consequently, a complex traffic intersection scenario was simulated, and the well-trained model was applied for driving control. The observed driving behavior closely resembled that of an experienced driver, exhibiting anticipatory actions and revealing notable operational highlights of driving policy.

Keywords

Autonomous Driving; Connected and Automated Vehicles; BEV-V2X; Trajectory Prediction; Decision-Making, Driving Planning and Control.

E-mail address: fli78@ford.com, nli26@ford.com.
Full postal address: *Ford Motor China Co.,ltd, Shanghai, 200082, China*

I. INTRODUCTION

Cooperative Intelligent Transport Systems (C-ITS) based on vehicle-to-everything (V2X) communication has considerably developed in recent years, bringing us closer to utilizing V2X for autonomous driving and assistance guidance [1-2]. Due to the numerous substantial benefits provided by C-ITS, governmental authorities worldwide have initiated the allocation of dedicated spectrum for V2X technologies, on a license-exempt basis in the 5.9 GHz band for the cellular based Cellular-V2X (C-V2X) PC5 technology [3-4].

The characteristics of 5G technologies including enhanced Mobile Broadband (eMBB) and massive Machine Type Communications (mMTC) are pivotal in vehicular communications [5-6]. Furthermore, facilitating Ultra-Reliable and Low-Latency Communications (URLLC) of 5G is a fundamental element of advanced V2X applications [7-8]. The application communication of PC5 in vehicle-to-vehicle (V2V) or infrastructure-to vehicle (V2I), as shown in Fig .1, results in quicker connections, reduced latency, enhanced reliability, increased capacity, and broader coverage, [9-11] significantly reducing issues caused by time asynchrony [12]. The spatial asynchrony challenges in V2X have seen an emergence of numerous solutions with the development of positioning and unified representation technologies [13-15]. Combining Global Navigation Satellite System (GNSS), real-time kinematics (RTK), Inertial Measurement Unit (IMU) and other vehicle sensors, multi-sensor fusion methodology has achieved lane-level positioning [16-19], significantly enhancing the real-time spatial positioning accuracy. Furthermore, the fusion misalignment arising from temporal, spatial asynchrony and limited wireless communication has been remarkably mitigated by Feature Flow Net (FFNet) [20]. These contributes to the matching of road links and lane to CAVs, along with the matching between road events, signs, traffic signals and CAVs using V2X.

Additionally, the fusion of perception and prediction in the V2I and V2V domains incorporating CAVs and roadside multi-sensor architectures has garnered heightened interest among researchers in the broader ITS-V2X field [21-23] . Infrastructure sensors, such as cameras and LiDARs, are often positioned at a greater height than the ego vehicles, affording them a wider field of view. The utilization of additional data from these infrastructure sensors can significantly enhance the acquisition of valuable information and enhance the perceptual capabilities of autonomous driving systems [24]. Many fusion frameworks for the data integration between

CAVs and infrastructure devices has been proposed for cooperative perception, forming comprehensive, precise, simultaneous fusion and prediction models for ITS-V2X [20, 25-27]. This advancement paves the way for the more precise and real-time enrichment of message sets (including MAP, SPAT, RSI, RSM, BSM) in V2X communication.

To facilitate the construction of maps and road network structures in crossroad areas, MAP enables the construction of maps for crossroad areas and establishes upstream and downstream road connectivity. SPAT information is harnessed to establish comprehensive insights into traffic signals based on signal phase and countdown, enabling synchronized traffic signal navigation. RSI data is utilized to delineate impact zones associated with road events and traffic signs, offering crucial information about obstacle positions and range information for the ego vehicle. Additionally, the utilization of time-stamped BSM data from multiple vehicles aids in ascertaining current vehicle positions, speeds, heading angles, and projecting future trajectories. These data provides a reliable and rich foundation for the subsequent prediction, decision-making, planning, and control in autonomous driving.

However, deploying untested algorithms directly onto a real autonomous-driving platform for road testing is known to be costly, time-consuming, and perilous. Hence, it is imperative to conduct thorough and reliable offline tests prior to the implementation of algorithms on an actual autonomous driving vehicle [28-30]. The research of cooperative driving relies heavily on the use of simulation and testing environments. Hardware-in-the-loop (HIL) simulation systems offer a cost-effective and efficient means of rapidly testing autonomous driving algorithms and hardware across a diverse range of virtual scenarios. Simulation experiments employing the HIL system serve to validate the effectiveness of autonomous driving algorithms in virtual environments, encompassing aspects like perception, planning, decision-making, and control [31].

The proposed HIL simulation system is composed of both infrastructure and ego CAV sides, which jointly form an integrated system for testing and verification in a closed-loop method.

The infrastructure side mainly includes three parts:

1) The virtual environment constructing software part, which simulates real traffic scenarios.

2) The V2X message sets generating software part, fusing perception and producing comprehensive V2X message sets.

3) The road side unit (RSU) hardware part, broadcasting and recivingV2X message sets using PC5 communication.

The ego CAV side also primarily contains three sections:

1) The In-Car System section including telematics control unit (TCU) and In-Vehicle Infotainment (IVI), which analyzes V2X message sets and display the location of real-time ego vehicle.

2) The controller model section, utilizing perception data, processing it into a BEV view and advanced data, and applying the EKF algorithm within an RL environment to perform trajectory prediction, decision-making, and driving control.

3) The on board unit (OBU) hardware part, receiving and sending V2X message sets using PC5 communication.

As shown in Fig.1, the whole figure demonstrates the HIL simulation process. The blue rectangle in the figure illustrates the simulated infrastructure side and the red rectangle exhibits the simulated ego CAV side.

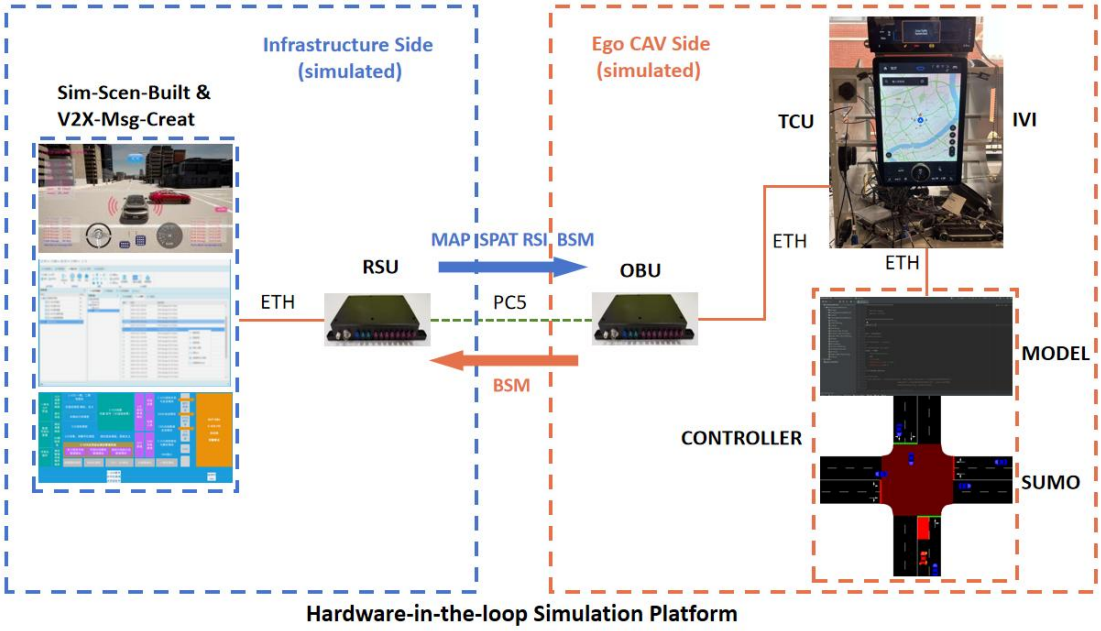

Fig. 1 the whole hardware-in-the-loop (HIL) simulation environment

In a simulation software stack that operates both on offline computers and in-vehicle systems, it encompasses interconnected components for simulating traffic scenarios, receiving V2X message sets and broadcasting between roadside and in-vehicle units, as well as conducting ego

vehicle driving planning and control. The software layer simulates perception data and vehicle states, forwarding them to core algorithms.

II. RELATED WORKS

A. BEV-V2X Perception

The objective of the perception module is to generate an intermediate-level representation of the environmental states (e.g., a bird's-eye view map displaying all obstacles and agents) that is to be subsequently employed by the decision-making system to formulate the driving policy. This representation encompasses lane positioning, drivable areas, the positions of other agents such as vehicles and pedestrians, as well as the status of traffic lights and other relevant factors. [32].

Bird-Eye-View (BEV) effectively presents the position and state of scenario elements in a concise and semantic way, relying on an occupancy grid as a foundation [33]. Typically, BEV is depicted as an image with a specific resolution, where each pixel corresponds to a predefined grid unit dimension [34]. BEV data include abundant semantic content, capable of amalgamating environmental details, road characteristics, and both the stationary and moving attributes of traffic participants [33]. A single BEV frame captures the driving state and relationships of all traffic participants at a specific timestamp in a particular road scenario, while a continuous sequence of BEV frames represents the driving behavior and interactions of these participants over a defined spatial and temporal range [35]. BEV data is of significance when it comes to creating a unified scenario representation across research areas like motion prediction [36-37], trajectory planning [38-39], and diving control [40-41].

However, establishing a real-time, precise, and globally semantic BEV has always been a challenge in the field of recognition.With the backing of PC5, allowing for quicker connections, reduced latency, and enhanced reliability, V2X communication significantly contributes to the realization of global BEV perception. This is made possible through the mature acquisition system with infrastructure sensors and the capacity for data fusion between infrastructure and vehicles [22]. There are essentially two primary communication modes for achieving BEV integration through Vehicle-to-Vehicle (V2V) and Vehicle-to-Infrastructure (V2I) communication in the context of V2X technology. Therefore, at the current stage, a substantial academic effort is concentrated on how to utilize V2X to efficiently and accurately integrate perception information from roadside infrastructure and Connected and Autonomous Vehicles (CAVs), rapidly

consolidating it into a comprehensive global BEV data for comprehensive environmental cognition around the vehicle. R Xu *et al.* [26] developed an all-encompassing attention model, referred to as V2X-ViT, to effectively combine data from various on-road entities, including vehicles and infrastructure, resulting in a remarkable advancement in 3D object detection as demonstrated by extensive empirical evidence. The essential components of V2X-ViT are structured within a cohesive Transformer framework, capable of addressing prevalent challenges in V2X applications, such as asynchronous information exchange, pose inaccuracies, and the diversity of V2X components. V2XFormer, as proposed by T Wang *et al.* [42], consists of extraction and alignment of multi-local BEV information, V2X fusion and task heads, outperforming the single-vehicle model in both perception and prediction tasks. This architecture empowers the transformation of raw sensory data from various vehicles, infrastructure and sensors into a consolidated BEV perception through V2X communication. Chang *et al.* [27] introduce a cooperative BEV fusion and prediction model called BEV-V2X to fuse and forecast the forthcoming global BEV occupancy grid map using the local BEV data collected from roadside unit or cloud center and data from all CAVs within a defined control area. Notably, BEV-V2X demonstrates a robust capability to accurately estimate and predict global spatial-temporal changes, even in scenarios where not all vehicles are CAVs.

Meanwhile, an increasing number of V2X-based BEV perception databases are being established to facilitate the availability of ample training and validation data for various scenarios and functionalities. Y Li *et al.* [43-44] create the V2X-Sim dataset by simulation, marking the first public large-scale collaborative perception dataset in the field of autonomous driving. This dataset offers synchronized BEV recordings from both roadside infrastructure and multiple vehicles at intersections, fostering collaborative perception capabilities. T Wang *et al.* [41] use CARLA realistic simulator to build the DeepAccident, a comprehensive dataset encompassing a wide range of accident scenarios commonly encountered in real-world driving. H Yu *et al.* [21] introduce the DAIR-V2X dataset derived from real scenarios, the initial extensive, multi-modal, multi-view dataset including LiDAR and camera frames captured in real-world scenes to support Vehicle-Infrastructure Cooperative Autonomous Driving (VICAD). All of these BEV-V2X fusion methods and associated datasets pave the path towards enhancing message sets (comprising MAP, SPAT, RSI, RSM, BSM) in V2X communication with greater precision and real-time updates.

B. Trajectory Prediction

Trajectory prediction is pivotal for CAVs to improve the safety by predicting the future conditions and states of ambient environment and other traffic participants. In particular, the representation of the anticipated movements of traffic participants through future trajectories is employed to proactively identify potential hazards, early warn vehicle collision and informs the development of decision-making and planning algorithms [45-48]. Therefore, the precise prediction of future paths taken by traffic participants is gaining considerable focus, emerging as an indispensable factor in enhancing the safety of autonomous driving systems.

Trajectory prediction challenges involve the formulation of utilizing the historical states of traffic participants within a specific scenario to estimate their forthcoming states. The states of traffic vehicles at the future times should be presented, commonly including the location, velocity and orientation of vehicles [46]. Prediction methods can be categorized into two main groups: physics-based methods, which encompass the Kalman filtering method and the Monte Carlo method, and neural network learning-based methods, including dynamic Bayesian network, deep learning-based method and reinforcement learning-based method [45], The trajectory prediction methods based on the Bayesian probability theory, such as the Kalman filter, have garnered significant attention due to their consideration of uncertainty and noise.

The future states of vehicle predicted is typically considered as imperfectly determined, subjected to inherent noise and interference derived from observational data [49-50]. The Kalman Filtering (KF) methods demonstrate proficiency in managing such noises by representing the uncertainty or noise associated with the current vehicle's state and its physical model through a Gaussian distribution [51]. Barrios, C *et al.* [52] introduced the KF to address inaccuracies associated with various potential states of a vehicle. By iteratively combining the prediction and update steps in a recursive loop, the mean value and covariance matrix for the vehicle's states can be relatively determined at multiple future time steps [53]. This process allows us to calculate a trajectory that is averaged while taking into account the related uncertainties [54]. Zhang *et al.* [55] conducted vehicle trajectory estimation and prediction using KF and vehicle-to-vehicle (V2V) communication to predict the coordinate, velocity and orientation of host vehicle (HV) and remote vehicle (RV). They apply the combined vehicle states of current time step and the two previous time steps to predict the vehicle states at the next time step, empowering HV with the capability to

anticipate and navigate around obstacles by predicting the trajectories of other RV. S. Ammoun *et al.* [53] predicted the trajectories with a temporal horizon of 10 seconds of both HV and RV using KF and a set of historical states of vehicles. The positions, velocities and accelerations of vehicles in two dimensions are utilized in the prediction step, while the vehicle's positions and velocities obtained through GPS receivers are used as measurement in the correction step. This approach is employed for trajectory prediction to facilitate the configuration of a vehicle collision model and the assessment of potential collision risks.

Indeed, the KF is a widely recognized recursive state estimator primarily designed for linear systems [56]. Nevertheless, its tracking precision may fall behind when confronted with non-linear scenarios, particularly in cases where the vehicle's velocity or acceleration undergo continuous variations. On this basis, several scholars have recommended filtering methods better tailored to address nonlinear systems. Jiang *et al.* [57] introduced the Extended Kalman Filter (EKF) approach for the estimation of the lateral state of an automobile, encompassing parameters such as speed, slip angle, acceleration. Alexander K [58] addressed both the lateral and longitudinal aspects of the vehicle's state. They introduced an adaptive fuzzy Extended Kalman Filter (EKF) - a state estimation technique rooted in the principles of the EKF to estimate the vehicle's dynamic characteristics. These above methods are capable of determining the vehicle's motion state through the utilization of vehicle kinematic principles, a fundamental requirement for most advanced intelligent vehicle control systems. H. Dyckmanns *et al.* [59] use EKF method to recognize and stable track the turning maneuver, enabling a stable tracking of longitudinal, crossing and turning traffic.

However, The EKF is exclusively suitable for systems exhibiting a moderate degree of non-linearity, given that it employs a strategy based on local linearization to approximate the global nonlinear model [60]. A number of scholars have explored the application of higher-order filters, such as second-order filters, to predict the future positions of vehicles, particularly to address the challenges posed by frequent changes in velocity or acceleration during real-world driving scenarios. The Unscented Kalman Filter (UKF), [61] as a method that approximates a Gaussian distribution rather than approximating a nonlinear function [62], has gained increasing attention due to its ability to maintain second-order accuracy while keeping computational costs low. Several studies [63-64] have employed the UKF as a substitute for the EKF in the task of

predicting the vehicle's state and addressing vehicle tracking challenges. The UKF algorithm offers improved practicality when compared to the EKF, as it avoids the potential truncation errors associated with Taylor expansion and obviates the requirement for solving the Jacobian matrix. H Wu *et al.* [65] combine two physics-based motion models, the constant velocity (CV) model and the coordinated turn (CT) model, utilizing the Interacting Multiple model (IMM)-UKF approach to attain precise motion estimation and prediction, resulting in a root mean square error (RMSE) of just 0.1 m in robot positioning. H Gao *et al.* [66] use the UKF filter to achieve high precision for vehicle maneuver trajectory prediction. These findings consistently demonstrate that UKF offers superior accuracy in the estimation of vehicle trajectories.

Moreover, vehicle trajectory prediction is inherently non-deterministic due to its dependence on various scenarios and their unpredictability [67], such as road curvature, driver's intention, phase and countdown of traffic lights, complex connectivity in junctions. Therefore, vehicle trajectory prediction is addressed using a range of motion models in several research strategies [68-71]. W. Blair [72] develops an innovative vehicle position prediction algorithm rooted in the constant velocity (CV) model. Zhang *et al.* [73] utilize constant acceleration (CA) model to develop kinematic positioning approach. In 1984, Professor Zhou [74] introduced the "current" statistical (CS) model, which posits that the change in target acceleration occurs within a vicinity centered around the acceleration value at the present time. On this basis, M. Deng *et al.* [75] proposed current statistical (CS) model and cubature Kalman filter (CKF) method to accurately predict the maneuver trajectory of vehicle.

Nevertheless, the situation becomes distinct when dealing with variable movement patterns. It provides high accuracy when a vehicle adheres to a consistent motion influenced by inertia [76-77]. However, it tends to yield inferior results in the long run, during emergency situations, and in complex traffic scenarios. Hence, utilizing Interacting Multiple model (IMM) and additional auxiliary information to assist real-time or predictive switching of motion models is a crucial endeavor for precise prediction. H Gao *et al.* [78] propose a IMM-UKF algorithm to achieve trajectory prediction with high accuracy for intelligent vehicles. Their IMM model combines the vehicle dynamics model, vehicle kinematics model, and maneuver recognition-based model using the UKF filter to achieve high precision. MT Abbas *et al.* [79] use the EKF with the integration of IMM, combined with constant velocity (CV) model, constant acceleration (CA)

model, vehicle turn (VT) model and other models, estimating the vehicle future location and trajectory up to 10 seconds. They also consider the effect between possibility of model switch for vehicle motion and the additional parameters, such as distance from the nearest intersection and turn signal.

Once a comprehensive range of potential scenarios and motion models for a vehicle has been established, probability density functions (PDFs) are subsequently computed. Among these PDFs, the model with the highest likelihood is chosen for predicting the future position of the vehicle. This entire process is executed by means of the IMM algorithm, which integrates the probabilities associated with each model through the utilization of a Markov model [17, 80]. Ultimately, a final transition metric is formulated, taking into account all the probabilities.

C. Decision-Making, Driving Planing and Control

By incorporating perceptions of all environmental states (including drivable areas, the positions of all vehicles and pedestrians , and the status of traffic lights), coupled with predictions of future trajectories for traffic participants, one can attempt to guide agents to model the uncertain interaction with environment and other traffic participants using decision-making and planning methods [81]. This approach forms the basis for driving strategies that prioritize safety and predictability within complex and cluttered traffic environments, such as intersections.

The agent faces the challenge of making real-time predictive decisions while navigating its surroundings after acquiring knowledge about novel environmental configurations. This challenge is amplified by a high dimensinal space given the number of unique configurations through which the agent and environment interact, resulting in a complex and combinatorially large problem. In these scenarios, our objective is to address a sequential decision-making process, a concept well-established in the field of Reinforcement Learning (RL). Within this framework, the agent is tasked with both acquiring an understanding of its environment and making optimal decisions in real-time. These optimal decisions are commonly referred to as 'policy'.

Reinforcement Learning (RL) holds significant promise, particularly within the domains of driving policy, path and motion planning, and the design of low-level controllers. The driving planning module plays a vital role in generating motion-level commands to steer the agent effectively. It's important to note that optimal planning, control, and reinforcement learning are intricately interconnected. In this context, optimal planning and control can be seen as a

model-based reinforcement learning problem, where the dynamics of the vehicle and its interaction with the environment are characterized by well-defined differential equations. Reinforcement learning methods have been developed to address stochastic decision-making and control problems as well as ill-posed challenges that involve unknown rewards and state transition probabilities [32].

Reinforcement learning facilitates model learning by allowing it to acquire task proficiency through a process of trial and error. This learning paradigm can be formally represented as a Markov decision process, formally described as a tuple (*S, A, P, R*), where *S* signifies the state space, *A* represents the action space of possible actions, *P* denotes the state transition probability model, and *R* characterizes the reward function. At each discrete time-step the agent observes a set of states s_t , takes an action a_t from the set of possible actions *A*, and subsequently, the environment undergoes a transition based on *P*. The agent then observes a new set of states s_{t+1} and receives a reward r_t . The goal of the agent is to learn a policy $\pi(s_t, a_t)$, which maps observations to actions in a way that maximizes the cumulative rewards. Consequently, the agent learns from its own actions during interactions with the environment and obtains an evaluation of its performance through the reward function [82].

Value-based algorithm is a category of RL algorithms, such as Q-learning [83], which focus on estimating the value function $V(s)$, representing the value (expected reward) associated with a specific state. When the state transition dynamics *P* are known, the policy can choose actions that lead to states where expected rewards are maximized. However, in many reinforcement learning scenarios, the environment model is unknown. In such cases, the state-action value or quality function $Q(s, a)$ is utilized instead. This function estimates the value of a particular action in a given state. The optimal policy is then determined by maximizing the state-action value function $Q(s, a)$ in a greedy way.

Deep learning provides numerous advantages when it comes to decision-making and planning. Its capacity to autonomously optimize behavior through data-driven adaptation to novel scenarios renders it highly compatible with control problems in complicated, dynamic environments [84-86]. The flexibility of deep learning empowers developers to instruct the system in performing proficiently and adapting to unfamiliar settings through the learning process [87-91].

This is why there has been a considerable surge in interest about the application of deep learning to autonomous driving planning and control in recent years.

Real-world scenarios also often involve continuous state and action spaces, which can be discretized. However, excessive discretization may limit performance, while fine-grained discretization can result in a large state-action space, making it impractical to gather enough samples for each pair. Alternatively, function approximation methods can be employed to generalize across states and actions. Function approximation is a dynamic field within RL, dealing with continuous state and action spaces, tackling state-action space complexities, and extending previous experiences to novel state-action pairs. Recent research has introduced deep neural networks as a function approximation method, leading to the emerging paradigm of deep reinforcement learning (DRL).

Deep Q-Networks (DQN) [87], a deep reinforcement learning algorithm, combines a variant of Q-learning algorithm with deep neural networks (DNNs). DNNs serve as a non-linear function approximator for state spaces of high dimension. The $Q(s, a)$ function is represented by a DNN that forecasts the value of all available actions based on the input state. Therefore, the process of determining the most suitable action involves executing a forward pass through the network. In additional, to enhance efficiency in utilizing samples, the agent's experiences are preserved within a replay memory (experience replay). Q-learning updates are then applied to samples chosen at random from this replay memory, and this random selection serves to disrupt the connections between consecutive samples. Experience replay empowers reinforcement learning agents to retain and reapply past experiences, where observed transitions are stored for a period, often in a queue, and uniformly sampled from this memory to update the network. For better robustness, DQN employs two networks where the parameters of the target network remain fixed for a set number of iterations before updates are made to the online network's parameters.

M Zhou *et.al* [92] proposed a DRL car following model based on Deep Deterministic Policy Gradient (DDPG), a combination of DQN and DPG. Their trained central controller can utilize the advantage of CAVs communicating with surrounding vehicles and traffic light systems to enhance travel efficiency, safety, and to reduce fuel consumption for CAVs when crossing signalized intersections. In order to reduce the computation time and realize collision-free driving, Y Guan *et.al* [93] develop a DRL algorithm called generalized exterior point (GEP) to find a neural

network solution offline. They transfer the decision-making and control problem under intersections to a process of optimal path selection and tracking, utilizing GEP to assist CAVs obtain approximate feasible optimal control policy. These authors [94-95] utilize Proximal Policy Optimization algorithm (PPO) to execute high-level decisions, trajectory and driving commands to infer ego vehicle-desired behavior in signalized and non-signalized traffic intersection.

D Isele *et.al* [96] conducted a comparative analysis between the Time-to-Collision (TTC) algorithm and the DQN algorithm, evaluating their capacity to acquire exploratory behaviors for navigating occluded intersections. Their findings indicate that DQN approaches demonstrate sound policies, successfully achieving the goal in 98.46% of instances within challenging scenarios, thus considerably outperforming other methods.

G Li *et.al* [97] utilize the deep Q-network algorithm to derive the optimal driving policy focused on both safety and efficiency. To verify the effectiveness of their decision-making framework, they simulate the top three intersection scenarios with a high risk of accidents involving crossing intersections. The results show that the method they developed could guide AVs to navigate intersections safely and efficiently in all the tested scenarios. The similar experiments and results can be seen in [98]. Some researchers [99] also propose a risk-aware DQN approach for decision making. They use a risk based reward function which punishes risky situations instead of only collision failures, learning more reliable policies which are safer in challenging situations.

T Tram *et.al* [100] employ DRQN [101] method, which combines a Long Short Term Memory (LSTM) with a DQN, for decision-making, planning and control purposes. This method is designed for automated vehicles that negotiate with other possibly non-automated vehicles in intersections, resulting in a significant lower collision to timeout ratio than previous algorithm.

Ⅲ. AN AUTONOMOUS DRIVING MODEL

A. BEV-V2X Perception

Road Connectivity:

Map

nodes: a list of intersections information

(1) **id**: the Id of this intersection
(1) **refPos**: 3D position of the center of this intersection,
including: latitude, longitude, elevation,
inLinks: a collection of directed roads connecting to this intersection
(2) **laneWidth**: the width of a single lane or a single inLink
(3) **name**: description about the relationship between nodes of this inLink
points: a list of midpoint vector points for current inLink
(4) **posOffset**: relative position deviation between refPos and points
offsetLL: the latitude and longitude deviation
offsetV: the elevation deviation
(5) **lanes**: a list of lanes information of this road
laneID: the Id of a single lane
points: a list of midpoint vector points for this lane
connectsTo: connectivity between current and downstream lane
(6) **connectinglane**: the data about downstream lanes
lane: the Id of downstream lane
maneuver: permitted types of turning
upstreamNodeId: the upstream intersection Id connected to this road

(1) refPos: (*lat, long*)
(2) laneWidth: *width*
(3) name: "*id1-id2*"
(4) points: [(*offset_lat, offset_long*), (...) ...]
(5) inLinks: {{name1, points, laneWidth}, {...}, ...} =
{{"*id1-id2*" [(*offset_lat, offset_long*) , (...) ...], *width*}, {...}, ...}
(6) → other inLinks: {...},{...},{...}

Transform to BEV and observation information:

1) refPos (*lat, long*) → O (x_o, y_o)
as the refPos is the center of the intersection, assume this as the origin O (0,0)
2) name "*id1-id2*" → inLinkName "*id1-id2*"
define the name of this inLink, implying from a node id to other node id.
3) points [(*offset_lat, offset_long*), (...) ...] → pointsinLink[(x_1, y_1), (...) ...]
4) inLink { "*id1-id2*", [(*offset_lat, offset_long*) , (...) ...], *width*} →
inLinkMap {"$id1 - id2$", [(x_1, y_1), $(\dots)$ $\dots$], $width$}
describe this inLink, including name, the coordinates of all points and occupied width
5) Other inLinks: {...},{...},{...} →inLinkMap(1){}, inLinkMap(2){}, inLinkMap(3){}
depict the contents of all downstream inLinks.

Other vehicles information

BSM

bsmFrame: the information of this traffic participant

(1)
- **id**: temporary vehicle Id
- **secMark**: the millisecond-level when this bsm message is transmitted
- **pos**: current 3D position of this traffic participant, including: elevation, latitude, longitude
- **speed**: the velocity of this traffic participant
- **heading**: the yaw angle of this traffic participant
- **size**: the size of this vehicle, including: width, length, height

(1) bsm [id: *vehicleId*, secMark: *timestamp*, pos(*lat, long*), speed: *velocity*, heading: *yaw angle*, size(*width, length*)]

Transform to BEV and observation information:

bsm [] → bsm

$[vehicleId, timestamp, (x^{vehicleId}, y^{vehicleId}), velocity, yaw\ angle, (width, length)]$

In the BEV representation, the lateral and longitudinal coordinates $(x^{vehicleId}, y^{vehicleId})$ of the vehicle define its center of gravity (considered as the center point in this paper). Subsequently, based on the *yaw angle*, *width*, and *length* of the vehicle, the maximum and minimum values for the occupied lateral and longitudinal coordinates $[x_{min}^{vehicleId}, x_{max}^{vehicleId}, y_{min}^{vehicleId}, y_{max}^{vehicleId}]$ are computed. The region encompassing these four extremities is then used to fill the vehicle grid occupancy in the BEV representation

Traffic Signal Light Information:

Map

nodes: a list of intersections information

- **id**: the Id of this intersection
- **inLinks**: a collection of directed roads connecting to this intersection

(3)
- **lanes**: a list of lanes information of the road

(1)
- **laneID**: the Id of the current single lane
- **connectsTo**: connectivity between current and downstream lane
- **phaseId**: traffic signal phase Id of this lane

- **movements**:a list of the signal phase Ids associated with this road connected here. Particularly, this phase Id is the unique linkage between the MAP message and the SPAT message

(2)
- **phaseId**: current traffic signal phase Id

(1) lane: (*laneId, phaseId1, phaseId2*)

(2) movements: (*phaseId1, phaseId2, phaseId3, ...*)

(3) inLinks: {[lane1, lane2, ...], movements} = {[(*laneId1, phaseId1, phaseId2*), (...), ...], (*phaseId1*, ...)}

Transform to BEV and observation information:

1) lane (*laneId, phaseId1, phaseId2*) → lane2phaseId (*laneId, phaseId1, phaseId2*)
   describe the relationship between lane and traffic light data (phase and countdown)
2) movements (*phaseId1, phaseId2*, ...) → phaseIdSet (*phaseId1, phaseId2*, ...)
   define a set including all phaseIds related to this current inLink.
3) inLink {[(*laneId1, phaseId1, phaseId2*), (...), ...], (*phaseId1*, ...)} →
   inLinkTL {[(*laneId1, phaseId1, phaseId2*), (...), ...], (*phaseId1*, ...)}
   depict this current inLink's information of all lanes and traffic light data, and its relationships.

SPAT

intersections: a list of intersections information

(4)
- **intersectionId**: the Id of this current intersection
- **moy**: UTC time in minutes
- **phases**: a list of the information of traffic signal phases

(3)
- **id**: this current phase id
- **phaseStates**: current states of this traffic signal phase

(2)
- **light**: description of this light, including: "v2i_green", "v2i_yellow", "v2i_red".
- **timing**: a signal phase status in countdown form

(1)
- **likelyEndTime**: the estimated time remaining from the current to the end of this phase
- **nextDuration**: the duration of time that will pass after next start of this phase state
- **startTime**: the time remaining until the start of this phase state from current moment

- **timeStamp**: milliseconds within a one-minute interval

(1) timing: (*endtime, nextduration, starttime*)
(2) phaseStates:{[light1, timing1], [...], [...]} =
{[*"v2i_green"*, timing1],[*"v2i_yellow"*, timing2],[*"v2i_red"*, timing3]}
(3) phases: {{*phaseId1*, phaseStates1}, {...}, ...}
(4) intersection{*intersectionId, moy, timeStamp,* phases} =
{*intersectionId, moy, timeStamp,* {{*phaseId1*, phaseStates1}, {...}, ...}}

Transform to BEV and observation information:

1) timing: (*endtime, nextduration, starttime*) →
   countdownTiming: (*endtime, nextduration, starttime*)
   describe the timing countdown information of the current phase state.
2) phaseStates:
   {[*"v2i_green"*, timing1], [*"v2i_yellow"*, timing2], [*"v2i_red"*, timing3]} →
   phaseStatesTL:
   {[*"v2i_green"*, countdownTiming1],
   [*"v2i_yellow"*,countdownTiming2],

[*"v2i_red"*, countdownTiming3]}

depict three timing states (green, yellow and red) of one traffic light phase

3) phases {{*phaseId1*, phaseStates1}, {...}, ...}
phasesTL {{*phaseId1*, phaseStatesTL1}, {...}, ...}
illustrate the relationship between phaseId and phaseState

4) intersection {*intersectionId, moy, timeStamp,* phases} →
intersectionTL {*intersectionId, moy, timeStamp,* phasesTL}
illustrate all traffic light information of this current intersection, including intersectionId, timestamp and all phases.

Road Event and Traffic Sign Information

RSI

RTS

(1) **refPos**: 3D position of the reference position, including: elevation, latitude, longitude
rtss: the information of this traffic sign (5)
rtsId: the Id of this rts information
signType: the type of this traffic sign
referencePaths: the associated alert path information for this traffic sign (4)
activePath: a directed coverage area information presented as an ordered list of position points (2)
offsetLL: the latitude and longitude deviation between refPos and this impact point
offsetV: the elevation deviation between refPos and this impact point
(3) **pathRadius**: the biggest distance away from the alert path within which the warning is active

(1) refPos: (*lat, long*)
(2) activePath: [(*offset_lat, offset_long*), (...), ...]
(3) pathRadius: *pathradius*
(4) referencePaths: {{activePath1, *pathradius1*}, {...}, ...} =
{{[(*offset_lat, offset_long*), (...), ...], *pathradius1*}, {...}, ...}
(5) rtss: {{*rtsId1*, referencePaths1}, {...}, ...}

Transform to BEV and observation information:

1) activePath [(*offset_lat, offset_long*), (...), ...] →
activePathPoints [(x^{rtsId}, y^{rtsId}), (...), ...]
describe a list of position points related to the impact area of this traffic sign

2) referencePaths {{activePath1, *pathradius1*}, {...}, ...} →
referencePathsArea {{activePathPoints1, *pathradius1*}, {...}, ...}
depict the associated path information for this traffic sign, including a list of position points and the impact path width (*pathradius*) away from these points.

3) rts: {*rtsId*, referencePaths} → rts: {*rtsId*, referencePathsArea}

illustrate the information of the traffic sign, including Id,.a list of position points and the impact path area of this traffic sign.

RTE

(1) **refPos**: 3D position of the reference position, including: elevation, latitude, longitude
rtes: a list of the information of road events
(4) **rteId**: the Id of this rte information
eventType: the type of this road event
eventSource: the event source
eventPos: the relative 3D positional deviation between refPos and the center of this event
(3) **offsetLL**: the latitude and longitude deviation
offsetV: the elevation deviation
(2) **eventRadius**: the impact range (radius) of this event

(1) refPos: (*lat, long*)
(2) eventRadius: *radius*
(3) eventPos: (*offset_lat, offset_long*)
(4) rtes: {[*rteId1*, eventPos1, *radius1*], [...], ...}

Transform to BEV and observation information:

rte: [*rteId*, (*offset_la1, offset_long*), *radius*] → rte: [*rteId1*, (x^{rteId}, y^{rtId}), *radius1*]
describe the information of the road event, including Id,.position and the impact radius of this event.

B. Trajectory Prediction

Algorithm 1 Immediate UKF Algorithm

Initialize:
(1) The initial mean state $\hat{x}_0$
(2) The initial covariance P_0
for *step_episode = 1, Max_steps* **do**
If *step_episode* $\neq$ *1*:
Observation and Validation:
(1) Calculate the observation vector $\hat{z}(t)$
(2) Calculate the validation region $\Phi_i(t, \varepsilon^2)$
(3) Calculate the innovation covariance $P_{zz}(t)$
Update:
(1) Calculate the near-optimal filter gain $K(t)$ and cross correlation $P_{xz}(t|t-1)$
(2) Update the estimated mean state $\hat{x}(t|t)$
(3) Update the error covariance $P_{xx}(t|t)$
Prediction:
(1) Predict the vehicle state $\hat{x}(t+1|t)$
(2) Predict the covariance matrix $P_{xx}(t+1|t)$
end

Algorithm 2 IMM Algorithm

for *step_episode = 1, Max_steps* **do**

Interaction:

(1) Calculate the mixing probability $\mu_{ij}(t+1)$

Model matched filtering:

(1) Calculate the initial state $\tilde{x}_j(t)$

(2) Calculate the associated mixing error covariance $\widetilde{P}_j(t)$

Model matched filtering:

(1) The probability update $\mu_i(t+1)$

Combination:

(1) Calculate the combined state $\hat{x}(t+1)$

(2) Calculate the associated mixing error covariance $P(t+1)$

end

$$X(t) = \left[x(t), y(t), v_x(t), v_y(t)\right]^T \tag{1}$$

$$U(t) = \left[\, a_x(t), a_y(t), \Delta\theta(t)\right]^T \tag{2}$$

$$X(t+1|t) = X(t|\,t) + f\big(X(t|\,t), U(t)\big) \tag{3}$$

1) Constant location model

$$U(t) = [0, 0, 0]^T$$

$$f\big(X(t|\,t), U(t)\big) = [0, 0, 0, 0]^T \tag{4}$$

2) Constant velocity model

$$U(t) = [0, 0, 0]^T$$

$$f\big(X(t|\,t), U(t)\big) = \left[v_x(t) \times \Delta T, v_y(t) \times \Delta T, 0, 0\right]^T \tag{5}$$

3) Constant acceleration model

$$U(t) = \left[a_x(t), a_y(t), \Delta\theta(t)\right]^T$$

$$f\big(X(t|\,t), U(t)\big) = \begin{pmatrix} v_x(t) \times \Delta T + 1/2 \times a_x(t) \times \Delta T^2 \\ v_y(t) \times \Delta T + 1/2 \times a_y(t) \times \Delta T^2 \\ a_x(t) \times \Delta T \\ a_y(t) \times \Delta T \end{pmatrix} \tag{6}$$

4) Constant jerk model

$$U(t) = \left[a_x(t) + j_x(t) \times \Delta T, a_y(t) + j_y(t) \times \Delta T, \Delta\theta(t)\right]^T$$

$$f\big(X(t|\,t),U(t)\big)=\begin{pmatrix} v_x(t)\times\Delta T+1/2\times a_x(t)\times\Delta T^2+1/6\times j_x(t)\times\Delta T^3 \\ v_y(t)\times\Delta T+1/2\times a_y(t)\times\Delta T^2+1/6\times j_y(t)\times\Delta T^3 \\ a_x(t)\times\Delta T+1/2\times j_x(t)\times\Delta T^2 \\ a_y(t)\times\Delta T+1/2\times j_y(t)\times\Delta T^2 \end{pmatrix} \tag{7}$$

5) Vehicle turn model

$$U(t)=[0,0,\Delta\theta(t)]^T$$

$$f\big(X(t|\,t),U(t)\big)=\begin{pmatrix} (v_x(t)\,cos\,(\Delta\theta(t))+v_y(t)\,sin\,(\Delta\theta(t)))\times\Delta T \\ (v_y(t)\,cos\,(\Delta\theta(t))-v_x(t)\,sin\,(\Delta\theta(t))\,)\times\Delta T \\ v_x(t)(cos\,(\Delta\theta(t))-1)+v_y(t)\,sin\,(\Delta\theta(t)) \\ v_y(t)(cos\,(\Delta\theta(t))-1)-v_x(t)\,sin\,(\Delta\theta(t)) \end{pmatrix} \tag{8}$$

Immediate UKF algorithm:

The information recursive update and prediction process must assess diverse uncertainty arising from both process noise and measurement noise. In this article, a Immediate UKF method is specifically designed to effectively manage the impact of noisy information and modeling errors.

Commencing with the representation of the discrete state transition equation of vehicle, considering uncertainty, the following equations are formulated:

$$X(t+1)=F[X(t),q(t),t]$$
$$Z(t)=H[X(t),w(t),t] \tag{9}$$

where $F[X(t)]$ and $q(t)$ represent the state function and process noise, respectively. And $H[X(t)]$ and $w(t)$ are the observation function and measurement noise, respectively.

1) Initialization: The initialization equations are written as follows:

$$\hat{x}_0=E[x_0]$$
$$P_0=E[(x_0-\hat{x}_0)(x_0-\hat{x}_0)^T] \tag{10}$$

where E is the mathematical expectation. Therefore, $\hat{x}_0$ is the mathematical expectation of x_0, and P_0 is the variance.

2) Prediction: The state transition equation of vehicle (3) is used to conduct state prediction and observation. The state prediction equation is formulated by instantiating each point to derive a set of transformed sigma points, as follows:

$$X_i(t+1|t)=F[X_i(t),U(t)],\quad i=0,\ldots,2L \tag{11}$$

where $F(\cdot)$ represents the state transition function.

The predicted vehicle state (predicated mean state) can be computed using:

$$\hat{x}(t+1|t) = \sum_{i=0}^{i=2L} W_i^m X_i(t+1|t) \quad (12)$$

The covariance of the state prediction is calculated according to:

$$P_{xx}(t+1|t) = \sum_{i=0}^{i=2L} W_i^c \{[X_i(t+1|t) - \hat{x}(t+1|t)] \times [X_i(t+1|t) - \hat{x}(t+1|t)]^T\} + Q(t|t) \quad (13)$$

where $Q(t|t)$ represents the covariance matrix of the process noise. Every element within the covariance matrix of process noise signifies the covariance among the errors of state elements, which can be examined based on the source of the errors.

This Immediate UKF approach is chosen to provide real-time predictions of the vehicle's state after receiving environmental data. Therefore, the UKF prediction step is employed to forecast the state for the next timestamp. Furthermore, upon receiving environmental data, a validation and update step is conducted on the previous vehicle state prediction before proceeding with the prediction of the state for the next timestamp, with details referring to the flowchart in Algorithm 1. This cyclic process is further detailed in the following two steps.

3) Observation and Validation: In each iteration of the immediate UKF process, this and next step is performed as a top priority. It involves the validation and update of the previous vehicle state prediction using the data received in the current step. For a detailed illustration of this procedure, please refer to the flowchart in Algorithm 1.

Each of the observation (measurement) point is instantiated as follows:

$$Z_i(t) = H[X_i(t)], \quad i = 0, \ldots, 2L \quad (14)$$

Then the observation mean can be obtained as:

$$\hat{z}(t) = \sum_{i=0}^{i=2L} W_i^m Z_i(t) \quad (15)$$

The validation region represents a critical threshold that is linked to the acceptability of observation values. It is crucial to emphasize that these values hold validity only when observation values fall within the validation region. Consequently, the validation region can be defined as follows:

$$\Phi_i(t, \varepsilon^2) = \{v: [Z_i(t) - \hat{z}(t)]^T \times [P_{zz}^i(t|t)]^{-1} \times [Z_i(t) - \hat{z}(t)] \leq \varepsilon^2\} \quad (16)$$

Where the threshold parameter ε corresponds to the number of sigma points. Additionally, opt for *2n + 1* sigma points, where *n* represents the dimension of the random variable. Given the additive and independent nature of measurement noise, the innovation covariance matrix is determined in the following equation:

$$P_{zz}(t) = \sum_{i=0}^{i=2L} W_i^c\{[Z_i(t) - \hat{z}(t)] \times [Z_i(t) - \hat{z}(t)]^T\} + R(t) \quad (17)$$

where $R(t)$ represents the covariance matrix of the measurement noise at current timestamp. The source of measuring noise covariance is the temporal and spatial asynchrony error when receiving BSMs message sets.

4) Update: The computation of near-optimal Kalman gain can be calculated as:

$$K(t) = P_{xz}(t|t-1) \times P_{zz}^{-1}(t) \quad (18)$$

with the cross correlation matrix:

$$P_{xz}(t|t-1) = \sum_{i=0}^{i=2L} W_i^c\{[X_i(t|t-1) - \hat{x}(t|t-1)] * [Z_i(t) - \hat{z}(t)]^T\} \quad (19)$$

The update information about the estimated mean state and the covariance matrix is, respectively:

$$\hat{x}(t|t) = \hat{x}(t|t-1) + K(t) \times (Z(t) - \hat{z}(t))$$
$$P_{xx}(t|t) = P_{xx}(t|t-1) + K(t) \times P_{zz}^{-1}(t) \times K(t)^T \quad (20)$$

IMM algorithm:

Due to the highly nonlinear nature of vehicle dynamics and the continuously changing behavior in complex traffic intersections, the choice of an appropriate control model combined with the trajectory prediction method is of utmost importance. In pursuit of this objective, an Interactive Multiple Model (IMM) algorithm is implemented, combining the Immediate UKF prediction approach and several control models to replace the solitary model only.

IMM can be characterized by the transition probabilities of the models at each iteration, offering a dependable solution for predicting trajectories during consistent changes in driving behavior. The IMM algorithm comprises four steps, outlined in Algorithm 2. The linear complexity of the IMM algorithm is evident from the number of iterations specified in the algorithm.

First, we define a set of five Immediate UKF models with different control module:

$$M = \{M_{CL}^{UKF}, M_{CV}^{UKF}, M_{CA}^{UKF}, M_{CJ}^{UKF}, M_{VT}^{UKF}\} \quad (21)$$

each control function of model has already been illustrated in the equations of (4-8)

Applying the Markov model, the probability of transitioning between states at a particular moment is only relied on its preceding state. It is assumed that for each timestamp, there exists a probability denoted as p_{ij}, signifying a transition from model *i* to model *j*, namely:

$$p_{ij} \triangleq p\big(M_j(t+1)\big|M_i(t)\big), \quad i,j \in \{CL, CV, CA, CJ, VT\} \quad (22)$$

where $0 < p_{ij} < 1$, and if i is certain, then the sum of p_{ij} over all j ($j \in \{CL, CV, CA, CJ, VT\}$) equals 1.

In the Markov model, given an initial state, subsequent to the transformation of the state transition matrix, the system will ultimately reach a stable state. This involves iteratively computing probability updates until a stable equilibrium state is attained. Assuming a prior of the probability for each model, namely, $\mu_r(0) = p(M_r(0)), r \in \{CL, CV, CA, CJ, VT\}$. The initial value of the probability transition matrix is utilized and subsequently computed iteratively according to Algorithm 2. The linear complexity of the IMM algorithm, as mentioned in previous research, implies that the probability transition matrix will converge to a certain value with minimal fluctuation. The resulting converged value represents the probability transition matrix.

1) Interaction: The IMM procedure initiates with the computation of the mixing probability for the interaction process. The normalized mixing probability $\mu_{ij}(t+1)$, derived from the probability transition matrix and the outcome of the preceding recursive probability $\mu_{ij}(t)$, is determined as follows:

$$\mu_{ij}(t+1) = \frac{1}{\bar{c}_j} p_{ij} \mu_i(t), \quad i, j \in \{CL, CV, CA, CJ, VT\} \tag{23}$$

with

$$\bar{c}_j = \sum_i p_{ij} \mu_i(t)$$

2) Model Matched Filtering: The calculation of the filter input is performed to estimate the initial mixing state $\tilde{x}_j(t)$ and the corresponding mixing error covariance $\tilde{P}_j(t)$ based on the mixing probability

$$\tilde{x}_j(t) = \sum_i \mu_{ij}(t) \hat{x}_i(t), \quad i, j \in \{CL, CV, CA, CJ, VT\}$$

$$\tilde{P}_j(t) = \sum_i \mu_{ij}(t) \left(P_i(t) + \left(\hat{x}_i(t) - \tilde{x}_j(t) \right) \left(\hat{x}_i(t) - \tilde{x}_j(t) \right)^T \right) \tag{24}$$

with

$$\left(\hat{x}_i(t+1), P_i(t+1) \right) = \mathcal{F}_i \left(\tilde{x}_i(t), \tilde{P}_i(t) \right)$$

where $\mathcal{F}_i(\cdot)$ represents the function of filter output for the model *i*. Meanwhile, $\hat{x}_i(t)$ and $P_i(t)$ are the filter output state and the associated covariance at timestamp *t*, respectively.

3) Model Probability Update: The probability update $\mu_i(t+1)$ for model *i* at timestamp $t+1$ can be deduced based on the likelihood function Λ_i as outlined below:

$$\mu_i(t+1) = \frac{1}{c} \Lambda_i(t+1) \bar{c}_i \tag{25}$$

with the normalization constant:

$$c = \sum_i \Lambda_i(t+1)\hat{x}_i(t+1) \tag{26}$$

4) Combination: The combined state $\hat{x}(t+1)$ and its covariance $\hat{P}(t+1)$ can be obtained as follow:

$$\hat{x}(t+1) = \sum_i \mu_j(t+1)\hat{x}_i(t+1), \quad i,j \in \{CL, CV, CA, CJ, VT\}$$

$$P(t+1) = \sum_i \mu_i(t+1) \times \{P_i(t+1) + [\hat{x}_i(t+1) - \hat{x}(t+1)] \times [\hat{x}_i(t+1) - \hat{x}(t+1)]^T\} \tag{27}$$

C. Driving Planning and Control

Kinematics Vehicle Model

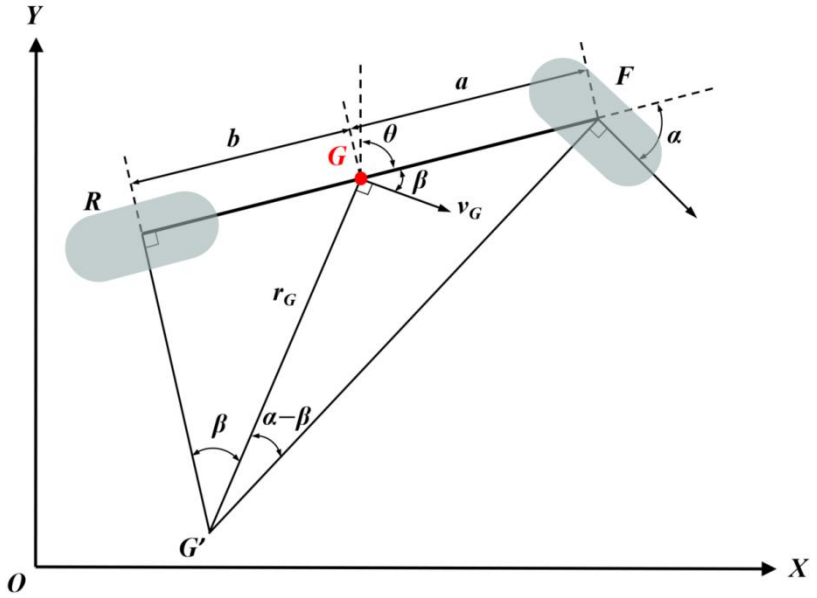

Fig. 2. “Bicycle” model

The "bicycle model" is a kinematic vehicle model illustrated in Figure 2. In this model, the traditional pairs of left and right wheels, both in the front and rear, are abstracted into two virtual wheels positioned in the middle of the vehicle. The steering angle of the front wheel is denoted as α, representing the angular difference between the vehicle's longitudinal axis and the orientation of the front wheel. The vehicle's center of gravity, designated as G, is located at distances a and b from the front and rear wheels, respectively. In the global coordinate frame, (x, y) signifies the coordinates of point G, while v_G represents the velocity vector located at point G. The angle θ denotes the yaw angle at last timestamp, and β characterizes the turn angle of the vehicle. Additionally, the line r_G corresponds to the radius of the vehicle's motion path, and the term $\bar{\theta} = \theta + \beta$ signifies the yaw angle at current timestamp.

By applying the "Sine Rule" to triangle G'GF and G'GR, the following equations can be easily derived:

$$\frac{sin\left(\frac{\pi}{2}-\alpha\right)}{r_G}=\frac{sin\,(\alpha-\beta)}{a},\qquad \frac{sin\left(\frac{\pi}{2}\right)}{r_G}=\frac{sin\,\beta}{b}. \tag{28}$$

Rearranging (28) leads to

$$tan\,\alpha\,cos\,\beta=\frac{a+b}{r_G} \tag{29}$$

Using (28) and (29), the turn angle β of vehicle can be obtained as

$$\beta=tan^{-1}\left(\frac{b\,tan\,\alpha}{a+b}\right) \tag{30}$$

Therefore, using (30) and the yaw angle at previous timestamp θ, the yaw angle at current timestamp $\bar{\theta}$ can be computed as

$$\bar{\theta}=\theta+\beta=\theta+tan^{-1}\left(\frac{b\,tan\,\alpha}{a+b}\right) \tag{31}$$

Dynamics Vehicle Model

The dynamics vehicle model would be transformed into a discrete vehicle motion model by employing the Euler implicit method, and the location of *G* represents the global coordinates of the vehicle (*x, y*). Specifically, if the action of ego vehicle is remain the state, which means continue the velocity and yaw angle at the last timestamp. The ego vehicle's position $(\bar{x},\bar{y})$, velocity $(\bar{v}_x,\bar{v}_y)$ and yaw angle $\bar{\theta}$ at the current timestamp can be computed as

$$\begin{pmatrix}\bar{x}\\ \bar{y}\\ \bar{v}_x\\ \bar{v}_y\\ \bar{\theta}\end{pmatrix}=\begin{pmatrix}x+v_G\,sin\,\theta\times\Delta T\\ y+v_G\,cos\,\theta\times\Delta T\\ v_G\,sin\,\theta\\ v_G\,cos\,\theta\\ \theta\end{pmatrix} \tag{32}$$

If the action of ego vehicle is accelerate or decelerate, and the acceleration is *a.* Then the velocity of ego vehicle at current timestamp $\bar{v}_G$ can be obtain as:

$$\bar{v}_G=v_G+a\times\Delta T \tag{33}$$

Combining (33), the ego vehicle's position $(\bar{x},\bar{y})$, velocity $(\bar{v}_x,\bar{v}_y)$ and yaw angle $\bar{\theta}$ at the current timestamp can be computed as

$$\begin{pmatrix}\bar{x}\\ \bar{y}\\ \bar{v}_x\\ \bar{v}_y\\ \bar{\theta}\end{pmatrix}=\begin{pmatrix}x+\bar{v}_G\,sin\,\theta\times\Delta T\\ y+\bar{v}_G\,cos\,\theta\times\Delta T\\ \bar{v}_G\,sin\,\theta\\ \bar{v}_G\,cos\,\theta\\ \theta\end{pmatrix} \tag{34}$$

If the action of ego vehicle is turn left or turn right, and the steering angle is α. Then combining (31) in the kinematic vehicle model, the ego vehicle's position $(\bar{x}, \bar{y})$, velocity $(\bar{v}_x, \bar{v}_y)$ and yaw angle $\bar{\theta}$ at the current timestamp can be obtained as

$$\begin{pmatrix} \bar{x} \\ \bar{y} \\ \bar{v}_x \\ \bar{v}_y \\ \bar{\theta} \end{pmatrix} = \begin{pmatrix} x + v_G \, sin\, \bar{\theta} \times \Delta T \\ y + v_G \cos \bar{\theta} \times \Delta T \\ v_G \, sin\, \bar{\theta} \\ v_G \cos \bar{\theta} \\ \theta + tan^{-1}\left(\frac{b \tan \alpha}{a+b}\right) \end{pmatrix} \tag{35}$$

Observation:

1) Relative position of goal (including shaped goals and the final goal)
2) Agent velocity
3) Agent yaw angle
4) Judgment of in-road
5) Distance to the lane line
6) Distance to the nearest position of off-road
7) Relative position to obstacle area
8) Relative position to the stop line of traffic signal light
9) Traffic signal light phase and countdown
10) At most ten other vehicles' driving states (relative position, velocity and yaw angle)
11) A current timestamp bird's-eye view gray-scale image with the agent at the center
12) A predicted next timestamp bird's-eye view gray-scale image with the agent at the center

Action:

1) Remain state (velocity and yaw angle)
2) Accelerate: acceleration a $= 1\ \mathrm{m/s^2}$
3) Decelerate: acceleration a $= -1\ \mathrm{m/s^2}$
4) Turn left : steering angle $\alpha = -\pi/6\ rad$
5) Turn right: steering angle $\alpha = \pi/6\ rad$

Reward: the reward is a weighted sum of the reward components shaped according to ego vehicle states, interactions involving surrounding vehicles, and key traffic events.

Reward Function:

$$Rewards \mathrel{+}= \begin{cases} -500 \text{ \& terminated} & \textit{if}: \text{driving in area of off-road, reverse-road and obstacle} \\ -500 \text{ \& terminated} & \textit{if}: \text{collision with other vehicles} \\ -500 \text{ \& terminated} & \textit{if}: \text{passing stop line during red light} \\ -500 \text{ \& terminated} & \textit{if}: \text{exceeding the } \textit{Max\_steps} \text{ without reaching final goal} \\ -100 & \textit{if}: \text{predicted agent collision or other dangerous events} \\ (200 - step\_episode) * \sqrt{shaped\_num\ +\ 1} & \textit{if}: \text{arriving at shaped goals} \\ -5 & \textit{if}: \text{occupied the lane line} \\ -1000 & \textit{if}: \text{terminated} \\ 1000 & \textit{if}: \text{arriving at the final goal} \\ -(acceleration)^2 * 10 & \textit{if}: \text{action is accelerate or decelerate} \end{cases} \tag{36}$$

Reward shaping method:

When applying DQN to address decision-making and driving planning problems in complex traffic environments, there is often a need for certain essential extensions of DRL. These extensions are aimed at enhancing the scalability, learning speed, and overall performance convergence of the algorithm within complicated problem domains.

Reward shaping is a common extension to improve the overall performance convergence of DRL environment and serves as a powerful mechanism for accelerating the learning speed of DRL agents by empirical evidence [102]. As is widely recognized, the formulation of the reward function holds a pivotal role in DRL. DRL agents are inherently driven to maximize their returns according to this reward function, thus serving as the basis for defining the optimal policy within a domain. In cases where a DRL agent may undergo a long period in discovering the objectives when learning from delayed rewards, the concept of shaping presents an opportunity to accelerate the learning process. The term "shaping" encompasses the notion of rewarding all behaviors that steer towards the desired actions. Through the method of reward shaping, it becomes possible to design a reward function that imparts more frequent feedback signals concerning suitable behaviors [103], a particularly valuable approach in domains with sparse rewards. In general, the adjustment of the return derived from the reward function is: $r' = r + f,$ where r represents the return from the original reward function R, f stands for the supplementary reward offered by a shaping function F, and r' denotes the signal provided to the agent via the expanded reward function R'.

The Fig. 3. illustrate the reward shaping design, where the yellow block represents the goals associated with the particular reward in reward function (36), including the shaped reward with shaped goals and the ultimate ones.

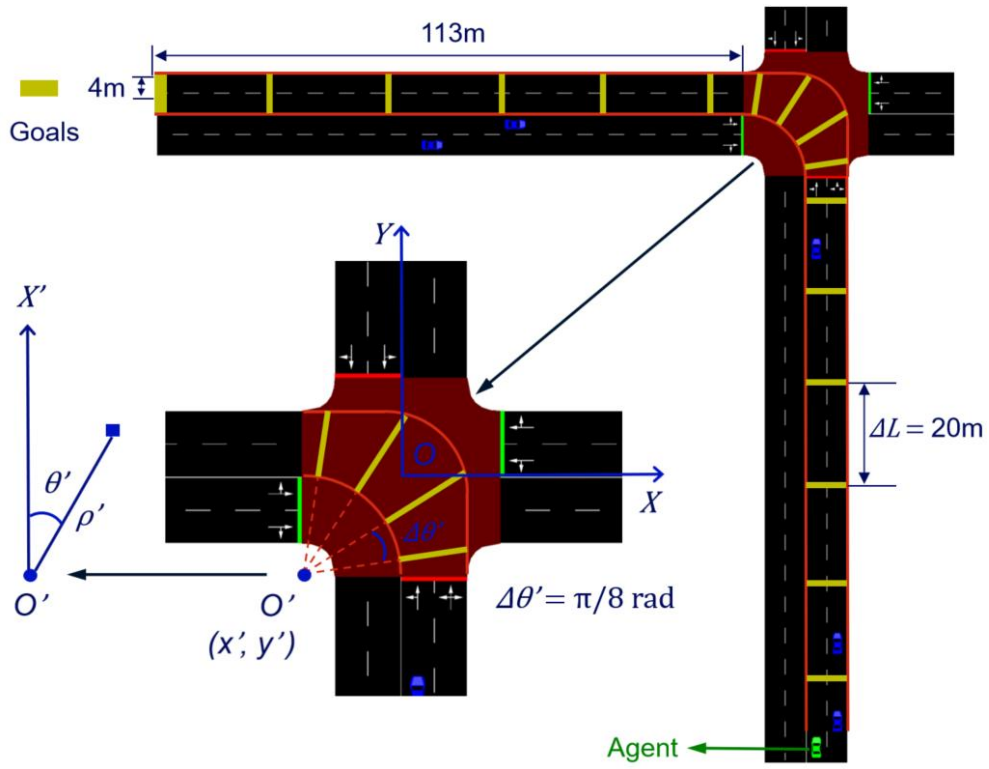

Fig. 3. the design of reward shaping for a DRL agent in traffic intersection

In the straight road, the shaped goals accompanied by shaped reward in (36) are separated and placed at fixed intervals of 20 meters, covering the whole width range of road. However, as the agent need maneuver turning left to arrive at the ultimate goal, the position and covering range of shaped goals in the intersection area should be expressed by polar coordinates. Then with the presentation of Fig. 3, the Cartesian - polar coordinates transformation in intersection can be computed as follow:

$$x' = x - w,\ y' = y - w$$
$$\rho' = \sqrt{x'^2 + y'^2}$$
$$\theta' = tan^{-1}(x'/y') \tag{37}$$

where (x, y) is the Cartesian coordinates in BEV presentation, (x', y') is the transformed coordinates for polar presentation, w is the half width of the center intersection area. Then the polar axis is oriented in the direction of a yaw angle of 0, which is the true north direction. And ρ' and θ' is the polar radius and the polar angle, respectively. Where $\theta' \epsilon (0, \pi/2)$, and when turning left, $\theta': \pi/2 \rightarrow 0$.

The covering range of can be divined into three phases according to the polar angle:

1st phase: when $\theta' \epsilon (0, \tan^{-1}(1/2))$, the minimum and maximum of radius can be computed as:

$$\rho'_{min} = w$$
$$\rho'_{max} = 2w/\cos\theta' \quad (38)$$

with $\theta' \epsilon (0, \tan^{-1}(1/2))$

2nd phase: when $\theta' \epsilon (\tan^{-1}(1/2), \tan^{-1}(2))$, the minimum and maximum of radius can be formulated as:

$$\rho'_{min} = w$$
$$\rho'_{max} = \sqrt{5}w \quad (39)$$

with $\theta' \epsilon (\tan^{-1}(1/2), \tan^{-1}(2))$

3rd phase: when $\theta' \epsilon (\tan^{-1}(2), \pi/2)$, the minimum and maximum of radius can be calculated as:

$$\rho'_{min} = w$$
$$\rho'_{max} = 2w/\sin\theta' \quad (40)$$

with $\theta' \epsilon (\tan^{-1}(2), \pi/2)$

In the center intersection area, combining the polar radius and polar angle in the equations (37-40), and the reward function (36), the shaped goals with shaped reward are divided and placed at fixed intervals of polar angle $\pi/8$, as shown in Fig. 3.

IV. TESTING RESULTS

In order to verify the effectiveness and performance of this autonomous driving model with interconnected functions, we conduct a series of simulation experiments. First, the BEV-V2X perception map was constructed. Subsequently, both the motion and occupancy predictions for all vehicles were accomplished. Finally, integrating the preceding works, a model was trained to complete driving decision-making and planning.

A. BEV-V2X Perception

The detailed diagram in Fig. 4 illustrates the establishment of road connectivity using the V2X (MAP) message set. It depicts the process of transforming the information required in the MAP messages from Section III.A into locally coordinated data. This process results in the construction of a global BEV perception map for road connectivity.

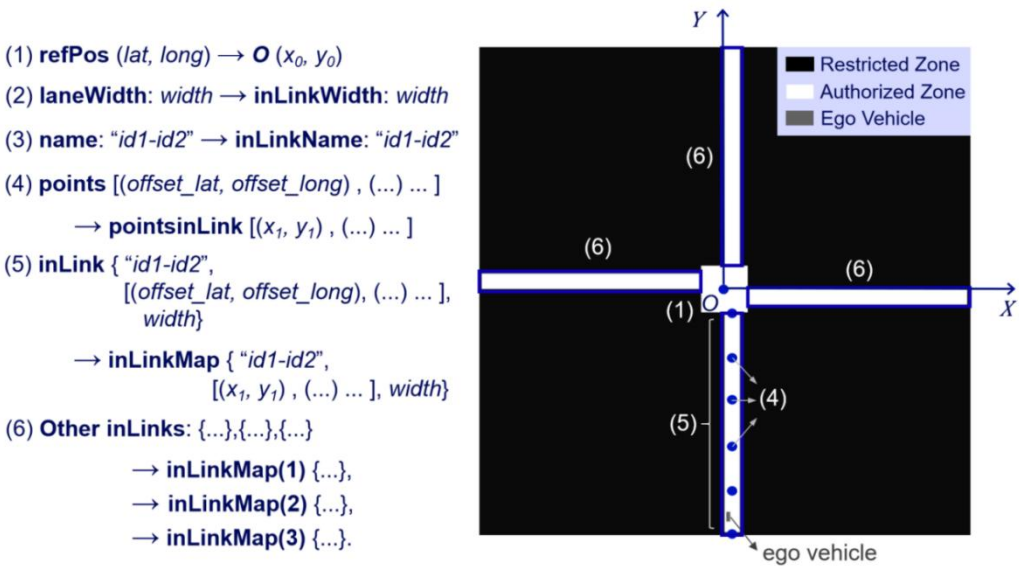

Fig. 4. Details on the construction for road connectivity

Subsequently, the constructed content of Traffic Signal Light Information, Road Event and Traffic Sign Information, and Other Vehicles Information from Section III.A is applied to the BEV local map. This results in a comprehensive map comprising authorized driving areas, occupancy regions by vehicles, dangerous areas, and traffic signal light information (utilizing the stop line to determine passage permission). The global BEV-V2X perception map is illustrated in Fig. 5.

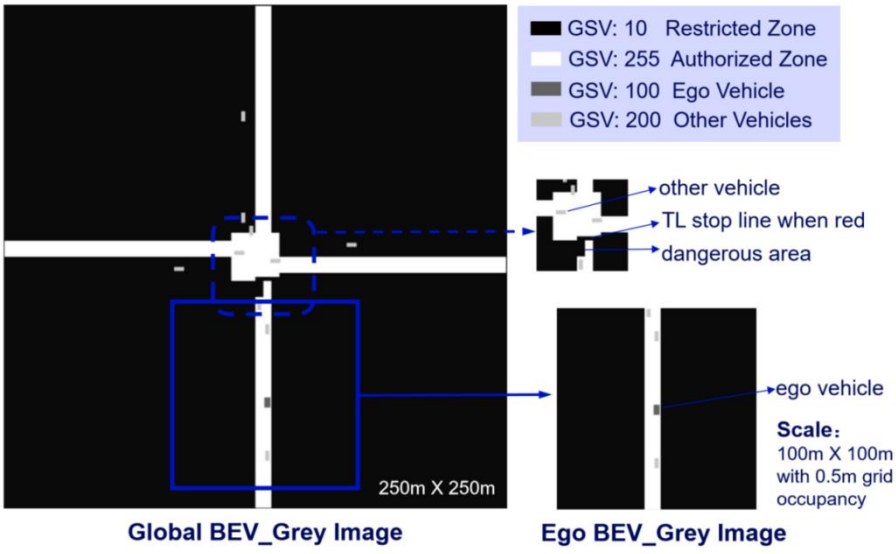

Fig. 5. BEV-V2X perception map

In Fig. 5, the BEV_Grey map utilizes different grayscale values to represent various elements, encompassing distinctive features of agents, other vehicles, and scene information. Subsequently, a local ego BEV_Grey map centered around the ego vehicle is segmented from the global BEV

map, serving as the input for perception data into the driving planning module for learning. The primary objective is to eliminate redundant information, accelerate convergence, and improve the training speed.

B. Motion and Occupancy Prediction

Applying the trajectory prediction method (IMM-UKF) from Section III.A, the real-time motion and occupancy predictions are conducted for all vehicles. Initially, the state information (position, velocity, heading angle, etc.) for all vehicles is used to predict their trajectories within a one-second, determining the vehicle's future state information. This information is then combined with the vehicle sizes to construct occupancy on the BEV_Grey map.

As shown in Fig. 6, the real-time motion and occupancy prediction for the left turning of the ego vehicle is depicted. The top row illustrates the actual ego vehicle grayscale map during the left turning process in the intersection. The second row represents the prediction map for all vehicles at each time point. The timestamps in each column of images are equal, with the upper images representing the actual BEV map and the lower images representing the predicted BEV map.

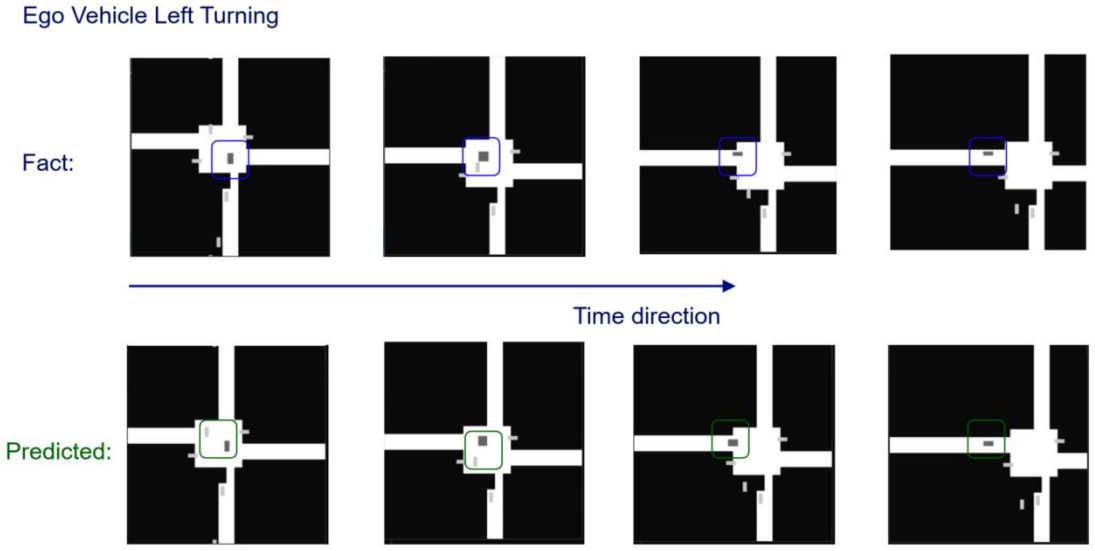

Fig. 6. The motion and occupancy prediction for ego vehicle left turning

Fig. 6 illustrates that through prediction, it is possible to proactively perceive the interactions between the ego vehicle and other vehicles or drivable areas. This enables anticipatory operations such as decelerating in advance, adjusting ego posture to avoid collisions, and providing a reference for proactive motions. Similarly, the predicted ego BEV_Grey map centered around the

ego vehicle is input into the driving planning module for training. This contributes to providing more valuable predictive information for interactive driving exploration and functionalities.

C. Decision Making and Planning

The driving decision-making and planning module adopts the approach from Section III.C, establishing a Deep Reinforcement Learning (DRL) environment. This involves incorporating perception and prediction information, road rules, and objectives into the reward and penalty functions for training the ego vehicle (agent), in planning and control.

During the inference process, the entire DRL model collaborates with SUMO software to enable the transmission of V2X information and showcase its outcomes. As depicted in Fig. 7, it illustrates the driving planning and control operations of the ego vehicle during the changing-lane phase on a straight road and the left-turning phase within an intersection, along with corresponding timestamps (blue), ego vehicle states (green), and action parameters (red) annotated in the Fig. 7.

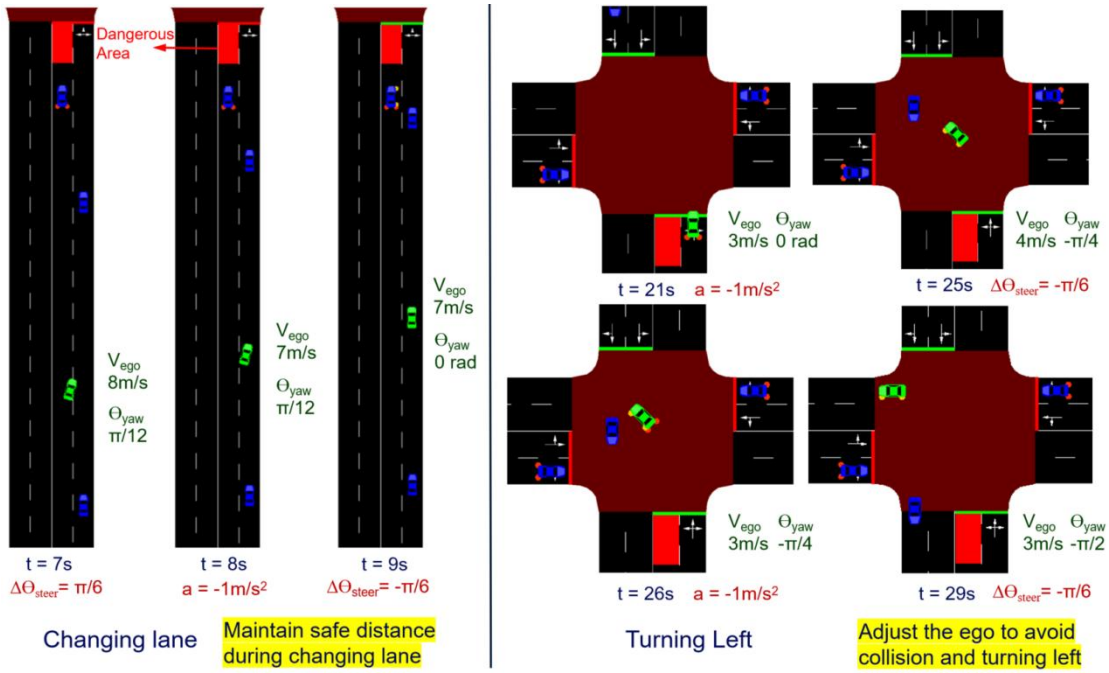

Fig. 7. The changing-lane phase and the left-turning phase of ego vehicle for driving planning results

During the lane-changing phase on the left side of Fig. 7, it can be observed that the ego vehicle, upon anticipating the presence of a non-navigable hazardous area ahead, decides to change lanes for overtaking. Prior to the lane change, it adjusts its speed to maintain a safe distance from fast and slow-moving vehicles in the adjacent lane. While changing lane, it initiates

a right turn, subsequently decelerates to ensure safety in posture and motion, and then completes the lane change with a left turn at the same angle. The entire process reflects anticipatory decision-making based on road conditions, showcasing a high level of driving planning safety.

The right side of Fig. 7 illustrates the left-turning phase within the intersection, involving operations such as navigating through a green light, continuous left turning, and making way for oncoming vehicles. Initially, the ego vehicle decelerates during the green light period, smoothly crosses the signal light stop line, and enters the intersection. Subsequently, it engages in continuous left turning by adjusting the overall posture through steering, acceleration, and deceleration. Anticipating and predicting the risk of collision with oncoming vehicles during the left turn, the ego vehicle proactively decelerates to avoid to the vehicles proceeding straight. Finally, it smoothly exits the intersection by consistently adjusting the vehicle's posture, completing the turning left operation. The entire process demonstrates the vehicle's intelligent navigation through driving planning, integrating perception and prediction. The interactive game planning and safety of the overall operation resemble an experienced human driver, showcasing a high level of driving planning intelligence.

V. FURTHER DISCUSSION

While this solution provides a comprehensive autonomous driving model, there is still much work to be done for improvement, including designing integrated learnable algorithms to enhance the efficiency and generalization, establishing interactive game predictions over long time intervals and testing the model using different datasets to validate its general effectiveness.

VI. CONCLUSIONS

This study presents an autonomous driving model that utilizes V2X-ITS perception data technology to construct a BEV perception map, employs IMM-UKF for motion and occupancy predictions of the ego and nearby vehicles, and establishes a DRL environment to train the agent for decision-making and driving planning. Finally, the model is trained and tested through the same dateset, presenting integrated driving behaviors that encompass obstacle avoidance, overtaking, lane changing, turning maneuver, and synchronized signal light navigation. This work provides a feasible and comprehensive solution for the research and application of connected intelligent vehicles (CAVs) using V2X technology in autonomous driving scenarios.

REFERENCES

[1] Wang, J.; Shao, Y.; Ge, Y.; Yu, R. A Survey of Vehicle to Everything (V2X) Testing. Sensors 2019, 19, 334. doi: 10.3390/s19020334

[2] Z. MacHardy, A. Khan, K. Obana and S. Iwashina, "V2X Access Technologies: Regulation, Research, and Remaining Challenges," in IEEE Communications Surveys & Tutorials, vol. 20, no. 3, pp. 1858-1877, thirdquarter 2018, doi: 10.1109/COMST.2018.2808444.

[3] V. Maglogiannis, D. Naudts, S. Hadiwardoyo, D. van den Akker, J. Marquez-Barja and I. Moerman, "Experimental V2X Evaluation for C-V2X and ITS-G5 Technologies in a Real-Life Highway Environment," in IEEE Transactions on Network and Service Management, vol. 19, no. 2, pp. 1521-1538, June 2022, doi: 10.1109/TNSM.2021.3129348.

[4] Costandoiu, A., and M. Leba. "Convergence of V2X communication systems and next generation networks." IOP Conference Series: Materials Science and Engineering. vol. 477. no. 1. IOP Publishing, 2019. doi: 10.1088/1757-899X/477/1/012052

[5] M. H. C. Garcia et al., "A Tutorial on 5G NR V2X Communications," in IEEE Communications Surveys & Tutorials, vol. 23, no. 3, pp. 1972-2026, thirdquarter 2021, doi: 10.1109/COMST.2021.3057017.

[6] K. Ganesan, P. B. Mallick, J. Löhr, D. Karampatsis and A. Kunz, "5G V2X Architecture and Radio Aspects," 2019 IEEE Conference on Standards for Communications and Networking (CSCN), Granada, Spain, 2019, pp. 1-6, doi: 10.1109/CSCN.2019.8931319.

[7] S. Chen et al., "Vehicle-to-Everything (v2x) Services Supported by LTE-Based Systems and 5G," in IEEE Communications Standards Magazine, vol. 1, no. 2, pp. 70-76, 2017, doi: 10.1109/MCOMSTD.2017.1700015.

[8] K. Sehla, T. M. T. Nguyen, G. Pujolle and P. B. Velloso, "Resource Allocation Modes in C-V2X: From LTE-V2X to 5G-V2X," in IEEE Internet of Things Journal, vol. 9, no. 11, pp. 8291-8314, 1 June1, 2022, doi: 10.1109/JIOT.2022.3159591.

[9] A. Alalewi, I. Dayoub and S. Cherkaoui, "On 5G-V2X Use Cases and Enabling Technologies: A Comprehensive Survey," in IEEE Access, vol. 9, pp. 107710-107737, 2021, doi: 10.1109/ACCESS.2021.3100472.

[10] R. Molina-Masegosa and J. Gozalvez, "LTE-V for Sidelink 5G V2X Vehicular Communications: A New 5G Technology for Short-Range Vehicle-to-Everything

Communications," in IEEE Vehicular Technology Magazine, vol. 12, no. 4, pp. 30-39, Dec. 2017, doi: 10.1109/MVT.2017.2752798.

[11] Dey, Kakan Chandra, et al. "Vehicle-to-vehicle (V2V) and vehicle-to-infrastructure (V2I) communication in a heterogeneous wireless network–Performance evaluation." Transportation Research Part C: Emerging Technologies 68, 2016: 168-184. doi:10.1016/j.trc.2016.03.008

[12] Kutila M, Kauvo K, Zheng Y, Zhang X, Garrido Martinez V. EU-China Joint V2X Trial Results. In Proceedings of the 2021 Joint European Conference on Networks and Communications & 6G Summit (EuCNC/6G Summit): Special Session 2 - EU-China Collaboration in 5G and Beyond. 2021

[13] Byun, Yeun-Sub, Rag-Gyo Jeong, and Seok-Won Kang. "Vehicle position estimation based on magnetic markers: Enhanced accuracy by compensation of time delays." Sensors 15.11, 2015: 28807-28825. doi: 10.3390/s151128807

[14] Byun, Yeun Sub, and Young Chol Kim. "Localization based on magnetic markers for an all-wheel steering vehicle." Sensors 16.12, 2016: 2015. doi: 10.3390/s16122015

[15] Yu, Haibao, et al. "Vehicle-infrastructure cooperative 3d object detection via feature flow prediction." arXiv preprint arXiv:2303.10552, 2023.

[16] Li, Tuan, et al. "High-accuracy positioning in urban environments using single-frequency multi-GNSS RTK/MEMS-IMU integration." Remote sensing 10.2, 2018: 205. doi: 10.3390/rs10020205

[17] Xu, Qimin, Xu Li, and Ching-Yao Chan. "A cost-effective vehicle localization solution using an interacting multiple model− unscented Kalman filters (IMM-UKF) algorithm and grey neural network." Sensors 17.6, 2017: 1431. doi: 10.3390/s17061431

[18] K. Jo, K. Chu and M. Sunwoo, "Interacting Multiple Model Filter-Based Sensor Fusion of GPS With In-Vehicle Sensors for Real-Time Vehicle Positioning," in IEEE Transactions on Intelligent Transportation Systems, vol. 13, no. 1, pp. 329-343, March 2012, doi: 10.1109/TITS.2011.2171033.

[19] Li, Xu, et al. "Multi-sensor fusion methodology for enhanced land vehicle positioning." Information Fusion 46, 2019: 51-62. doi: 10.1016/j.inffus.2018.04.006

[20] Yu, Haibao, et al. "Vehicle-infrastructure cooperative 3d object detection via feature flow prediction." arXiv preprint arXiv:2303.10552, 2023.

[21] Yu, Haibao, et al. "Dair-v2x: A large-scale dataset for vehicle-infrastructure cooperative 3d object detection." Proceedings of the IEEE/CVF Conference on Computer Vision and Pattern Recognition. 2022.

[22] Fan, Siqi, et al. "Quest: Query stream for vehicle-infrastructure cooperative perception." arXiv preprint arXiv:2308.01804, 2023.

[23] Yu, Haibao, et al. "V2X-Seq: A Large-Scale Sequential Dataset for Vehicle-Infrastructure Cooperative Perception and Forecasting." Proceedings of the IEEE/CVF Conference on Computer Vision and Pattern Recognition. 2023.

[24] E. Guo, Z. Chen, S. Rahardja and J. Yang, "3D Detection and Pose Estimation of Vehicle in Cooperative Vehicle Infrastructure System," in IEEE Sensors Journal, vol. 21, no. 19, pp. 21759-21771, 1 Oct.1, 2021, doi: 10.1109/JSEN.2021.3101497.

[25] Hu, Yue, et al. "Where2comm: Communication-efficient collaborative perception via spatial confidence maps." Advances in neural information processing systems 35, 2022: 4874-4886.

[26] Xu, Runsheng, et al. "V2x-vit: Vehicle-to-everything cooperative perception with vision transformer." European conference on computer vision. Cham: Springer Nature Switzerland, 2022. doi: 10.1007/978-3-031-19842-7_7

[27] C. Chang et al., "BEV-V2X: Cooperative Birds-Eye-View Fusion and Grid Occupancy Prediction via V2X-Based Data Sharing," in IEEE Transactions on Intelligent Vehicles, doi: 10.1109/TIV.2023.3293954.

[28] G. Ros, S. Ramos, M. Granados, A. Bakhtiary, D. Vazquez and A. M. Lopez, "Vision-Based Offline-Online Perception Paradigm for Autonomous Driving," 2015 IEEE Winter Conference on Applications of Computer Vision, Waikoloa, HI, USA, 2015, pp. 231-238, doi: 10.1109/WACV.2015.38.

[29] J. Florbäck, L. Tornberg and N. Mohammadiha, "Offline object matching and evaluation process for verification of autonomous driving," 2016 IEEE 19th International Conference on Intelligent Transportation Systems (ITSC), Rio de Janeiro, Brazil, 2016, pp. 107-112, doi: 10.1109/ITSC.2016.7795539.

[30] S. Chen, J. Shang, S. Zhang and N. Zheng, "Cognitive map-based model: Toward a developmental framework for self-driving cars," 2017 IEEE 20th International Conference on

Intelligent Transportation Systems (ITSC), Yokohama, Japan, 2017, pp. 1-8, doi: 10.1109/ITSC.2017.8317627.

[31] S. Chen, Y. Chen, S. Zhang and N. Zheng, "A Novel Integrated Simulation and Testing Platform for Self-Driving Cars With Hardware in the Loop," in IEEE Transactions on Intelligent Vehicles, vol. 4, no. 3, pp. 425-436, Sept. 2019, doi: 10.1109/TIV.2019.2919470.

[32] B. R. Kiran et al., "Deep Reinforcement Learning for Autonomous Driving: A Survey," in IEEE Transactions on Intelligent Transportation Systems, vol. 23, no. 6, pp. 4909-4926, June 2022, doi: 10.1109/TITS.2021.3054625.

[33] Li, Zhiqi, et al. "Bevformer: Learning bird ' s-eye-view representation from multi-camera images via spatiotemporal transformers." European conference on computer vision. Cham: Springer Nature Switzerland, 2022. doi: 10.1007/978-3-031-20077-9_1

[34] Roddick, Thomas, and Roberto Cipolla. "Predicting semantic map representations from images using pyramid occupancy networks." Proceedings of the IEEE/CVF Conference on Computer Vision and Pattern Recognition. 2020.

[35] C. Chang et al., "MetaScenario: A Framework for Driving Scenario Data Description, Storage and Indexing," in IEEE Transactions on Intelligent Vehicles, vol. 8, no. 2, pp. 1156-1175, Feb. 2023, doi: 10.1109/TIV.2022.3215503.

[36] Fang, Liangji, et al. "Tpnet: Trajectory proposal network for motion prediction." Proceedings of the IEEE/CVF Conference on Computer Vision and Pattern Recognition. 2020. doi: 10.48550/arXiv.2004.12255

[37] V. Lefkopoulos, M. Menner, A. Domahidi and M. N. Zeilinger, "Interaction-Aware Motion Prediction for Autonomous Driving: A Multiple Model Kalman Filtering Scheme," in IEEE Robotics and Automation Letters, vol. 6, no. 1, pp. 80-87, Jan. 2021, doi: 10.1109/LRA.2020.3032079.

[38] Y. Guo, D. Yao, B. Li, H. Gao, and L. Li, "Down-Sized Initialization for Optimization-Based Unstructured Trajectory Planning by Only Optimizing Critical Variables," IEEE Transactions on Intelligent Vehicles, vol. 8, no. 1, pp. 709-720, 2023.

[39] Hu, Yihan, et al. "Planning-oriented autonomous driving." Proceedings of the IEEE/CVF Conference on Computer Vision and Pattern Recognition. 2023. doi: 10.48550/arXiv.2212.10156

[40] Lillicrap, Timothy P., et al. "Continuous control with deep reinforcement learning." arXiv preprint arXiv:1509.02971, 2015. doi: 10.48550/arXiv.1509.02971

[41] H. Porav and P. Newman, "Imminent Collision Mitigation with Reinforcement Learning and Vision," 2018 21st International Conference on Intelligent Transportation Systems (ITSC), Maui, HI, USA, 2018, pp. 958-964, doi: 10.1109/ITSC.2018.8569222.

[42] Wang, Tianqi, et al. "DeepAccident: A Motion and Accident Prediction Benchmark for V2X Autonomous Driving." arXiv preprint arXiv:2304.01168, 2023. doi: 10.48550/arXiv.2304.01168

[43] Li, Yiming, et al. "V2x-sim: A virtual collaborative perception dataset for autonomous driving." arXiv preprint arXiv:2202.08449, 2022.

[44] Y. Li et al., "V2X-Sim: Multi-Agent Collaborative Perception Dataset and Benchmark for Autonomous Driving," in IEEE Robotics and Automation Letters, vol. 7, no. 4, pp. 10914-10921, Oct. 2022, doi: 10.1109/LRA.2022.3192802.

[45] Y. Huang, J. Du, Z. Yang, Z. Zhou, L. Zhang and H. Chen, "A Survey on Trajectory-Prediction Methods for Autonomous Driving," in IEEE Transactions on Intelligent Vehicles, vol. 7, no. 3, pp. 652-674, Sept. 2022, doi: 10.1109/TIV.2022.3167103.

[46] F. Leon and M. Gavrilescu, "A review of tracking and trajectory prediction methods for autonomous driving," Mathematics, vol. 9, no. 6, pp. 660 – 696, 2021. doi: 10.3390/math9060660

[47] S. Mozaffari, O. Y. Al-Jarrah, M. Dianati, P. Jennings and A. Mouzakitis, "Deep Learning-Based Vehicle Behavior Prediction for Autonomous Driving Applications: A Review," in IEEE Transactions on Intelligent Transportation Systems, vol. 23, no. 1, pp. 33-47, Jan. 2022, doi: 10.1109/TITS.2020.3012034.

[48] J. Liu, X. Mao, Y. Fang, D. Zhu, and M. Q.-H. Meng, "A survey on deep-learning approaches for vehicle trajectory prediction in autonomous driving," in Proc. IEEE Int. Conf. Robot. Biomim., 2021, pp. 978–985, doi: 10.1109/ROBIO54168.2021.9739407.

[49] B. Paden, M. ˇCáp, S. Z. Yong, D. Yershov, and E. Frazzoli, "A survey of motion planning and control techniques for self-driving urban vehicles,"IEEE Trans. Intell. Veh., vol. 1, no. 1, pp. 33–55, Mar. 2016.

[50] S. Lefèvre, D. Vasquez, and C. Laugier, "A survey on motion prediction and risk assessment for intelligent vehicles, " ROBOMECH J., vol. 1, no. 1, pp. 1 – 14, 2014. doi: 10.1186/s40648-014-0001-z

[51] N. Kaempchen, K. Weiss, M. Schaefer and K. C. J. Dietmayer, "IMM object tracking for high dynamic driving maneuvers," IEEE Intelligent Vehicles Symposium, 2004, Parma, Italy, 2004, pp. 825-830, doi: 10.1109/IVS.2004.1336491.

[52] C. Barrios and Y. Motai, "Improving Estimation of Vehicle's Trajectory Using the Latest Global Positioning System With Kalman Filtering," in IEEE Transactions on Instrumentation and Measurement, vol. 60, no. 12, pp. 3747-3755, Dec. 2011, doi: 10.1109/TIM.2011.2147670.

[53] S. Ammoun and F. Nashashibi, "Real time trajectory prediction for collision risk estimation between vehicles," 2009 IEEE 5th International Conference on Intelligent Computer Communication and Processing, Cluj-Napoca, Romania, 2009, pp. 417-422, doi: 10.1109/ICCP.2009.5284727.

[54] T. Batz, K. Watson and J. Beyerer, "Recognition of dangerous situations within a cooperative group of vehicles," 2009 IEEE Intelligent Vehicles Symposium, Xi'an, China, 2009, pp. 907-912, doi: 10.1109/IVS.2009.5164400.

[55] Zhang, Ruifeng, et al. "A method for connected vehicle trajectory prediction and collision warning algorithm based on V2V communication." International Journal of Crashworthiness 22.1, 2017: 15-25. doi: 10.1080/13588265.2016.1215584

[56] Kalman, Rudolph Emil. "A new approach to linear filtering and prediction problems." Journal of basic Engineering 82.1 (1960): 35-45.

[57] K. Jiang, A. C. Victorino and A. Charara, "Real-time estimation of vehicle's lateral dynamics at inclined road employing extended Kalman filter," 2016 IEEE 11th Conference on Industrial Electronics and Applications (ICIEA), Hefei, China, 2016, pp. 2360-2365, doi: 10.1109/ICIEA.2016.7603987.

[58] A. Katriniok and D. Abel, "Adaptive EKF-Based Vehicle State Estimation With Online Assessment of Local Observability," in IEEE Transactions on Control Systems Technology, vol. 24, no. 4, pp. 1368-1381, July 2016, doi: 10.1109/TCST.2015.2488597.

[59] H. Dyckmanns, R. Matthaei, M. Maurer, B. Lichte, J. Effertz and D. Stüker, "Object tracking in urban intersections based on active use of a priori knowledge: Active interacting multi model filter," 2011 IEEE Intelligent Vehicles Symposium (IV), Baden-Baden, Germany, 2011, pp. 625-630, doi: 10.1109/IVS.2011.5940443.

[60] Lefebvre*, Tine, Herman Bruyninckx, and Joris De Schutter. "Kalman filters for non-linear systems: a comparison of performance." International journal of Control 77.7, 2004: 639-653. doi: 10.1080/00207170410001704998

[61] E. A. Wan and R. Van Der Merwe, "The unscented Kalman filter for nonlinear estimation," Proceedings of the IEEE 2000 Adaptive Systems for Signal Processing, Communications, and Control Symposium (Cat. No.00EX373), Lake Louise, AB, Canada, 2000, pp. 153-158, doi: 10.1109/ASSPCC.2000.882463.

[62] Julier, Simon J., and Jeffrey K. Uhlmann. "New extension of the Kalman filter to nonlinear systems." Signal processing, sensor fusion, and target recognition VI. Vol. 3068. Spie, 1997. doi: 10.1117/12.280797

[63] J. Li, M. Ye, S. Jiao, W. Meng and X. Xu, "A Novel State Estimation Approach Based on Adaptive Unscented Kalman Filter for Electric Vehicles," in IEEE Access, vol. 8, pp. 185629-185637, 2020, doi: 10.1109/ACCESS.2020.3030260.

[64] Wang, Yu, Yushan Li, and Ziliang Zhao. "State Parameter Estimation of Intelligent Vehicles Based on an Adaptive Unscented Kalman Filter." Electronics 12.6, 2023: 1500. doi: 10.3390/electronics12061500

[65] Wu, Hao, et al. "Interacting multiple model-based adaptive trajectory prediction for anticipative human following of mobile industrial robot." Procedia Computer Science 176 2020: 3692-3701.doi: 10.1016/j.procs.2020.09.330

[66] H. Gao, Y. Qin, C. Hu, Y. Liu and K. Li, "An Interacting Multiple Model for Trajectory Prediction of Intelligent Vehicles in Typical Road Traffic Scenario," in IEEE Transactions on Neural Networks and Learning Systems, vol. 34, no. 9, pp. 6468-6479, Sept. 2023, doi: 10.1109/TNNLS.2021.3136866.

[67] J. Quehl, H. Hu, S. Wirges and M. Lauer, "An Approach to Vehicle Trajectory Prediction Using Automatically Generated Traffic Maps," 2018 IEEE Intelligent Vehicles Symposium (IV), Changshu, China, 2018, pp. 544-549, doi: 10.1109/IVS.2018.8500535.

[68] Y. Hu, W. Zhan and M. Tomizuka, "Probabilistic Prediction of Vehicle Semantic Intention and Motion," 2018 IEEE Intelligent Vehicles Symposium (IV), Changshu, China, 2018, pp. 307-313, doi: 10.1109/IVS.2018.8500419.

[69] D. Jeong, M. Baek and S. -S. Lee, "Long-term prediction of vehicle trajectory based on a deep neural network," 2017 International Conference on Information and Communication Technology Convergence (ICTC), Jeju, Korea (South), 2017, pp. 725-727, doi: 10.1109/ICTC.2017.8190764.

[70] N. Suganuma and T. Uozumi, "Precise position estimation of autonomous vehicle based on map-matching," 2011 IEEE Intelligent Vehicles Symposium (IV), Baden-Baden, Germany, 2011, pp. 296-301, doi: 10.1109/IVS.2011.5940510.

[71] Hoshizaki T. Method and apparatus to estimate vehicle position and recognized landmark positions using GPS and camera. US patent 7,868,821. January 11, 2011.

[72] W. D. Blair, "Design of nearly constant velocity filters for radar tracking of maneuvering targets," 2012 IEEE Radar Conference, Atlanta, GA, USA, 2012, pp. 1008-1013, doi: 10.1109/RADAR.2012.6212285.

[73] Zhang, Kaishi, et al. "Smart-RTK: Multi-GNSS kinematic positioning approach on android smart devices with Doppler-smoothed-code filter and constant acceleration model." Advances in Space Research 64.9, 2019: 1662-1674. doi: 10.1016/j.asr.2019.07.043

[74] Zhou, Hongren, and K. S. P. Kumar. "A'current'statistical model and adaptive algorithm for estimating maneuvering targets." Journal of guidance, control, and dynamics 7.5, 1984: 596-602. doi.org/10.2514/3.19900

[75] Deng, Mingjun, et al. "Vehicle Trajectory Prediction Method Based on “Current” Statistical Model and Cubature Kalman Filter." Electronics 12.11, 2023: 2464. doi: 10.3390/electronics12112464

[76] A. Berthelot, A. Tamke, T. Dang and G. Breuel, "Handling uncertainties in criticality assessment," 2011 IEEE Intelligent Vehicles Symposium (IV), Baden-Baden, Germany, 2011, pp. 571-576, doi: 10.1109/IVS.2011.5940483.

[77] A. Tamke, T. Dang and G. Breuel, "A flexible method for criticality assessment in driver assistance systems," 2011 IEEE Intelligent Vehicles Symposium (IV), Baden-Baden, Germany, 2011, pp. 697-702, doi: 10.1109/IVS.2011.5940482.

[78] H. Gao, Y. Qin, C. Hu, Y. Liu and K. Li, "An Interacting Multiple Model for Trajectory Prediction of Intelligent Vehicles in Typical Road Traffic Scenario," in IEEE Transactions on Neural Networks and Learning Systems, vol. 34, no. 9, pp. 6468-6479, Sept. 2023, doi: 10.1109/TNNLS.2021.3136866.

[79] Abbas, Muhammad Tahir, et al. "An adaptive approach to vehicle trajectory prediction using multimodel Kalman filter." Transactions on Emerging Telecommunications Technologies 31.5, 2020: e3734. doi.org/10.1002/ett.3734

[80] K. Jo, K. Chu and M. Sunwoo, "Interacting Multiple Model Filter-Based Sensor Fusion of GPS With In-Vehicle Sensors for Real-Time Vehicle Positioning," in IEEE Transactions on Intelligent Transportation Systems, vol. 13, no. 1, pp. 329-343, March 2012, doi: 10.1109/TITS.2011.2171033.

[81] Schwarting, Wilko, Javier Alonso-Mora, and Daniela Rus. "Planning and decision-making for autonomous vehicles." Annual Review of Control, Robotics, and Autonomous Systems 1 2018: 187-210. doi: 10.1146/annurev-control-060117-105157

[82] Z. Wang et al., " Sample efficient actor-critic with experience replay, " 2016, arXiv:1611.01224. [Online]. Available: https://arxiv.org/ abs/1611.01224

[83] Devraj, Adithya M., and Sean P. Meyn. "Fastest convergence for Q-learning." arXiv preprint arXiv:1707.03770, 2017. doi: 10.48550/arXiv.1707.03770

[84] S. Levine, C. Finn, T. Darrell, and P. Abbeel, "End-to-end training of deep visuomotor policies," J. Mach. Learn. Res., vol. 17, no. 1, pp. 1334–1373, 2015.

[85] Levine, Sergey, et al. "Learning hand-eye coordination for robotic grasping with deep learning and large-scale data collection." The International journal of robotics research 37.4-5 (2018): 421-436. doi: 10.1177/02783649177103

[86] V. Rausch, A. Hansen, E. Solowjow, C. Liu, E. Kreuzer and J. K. Hedrick, "Learning a deep neural net policy for end-to-end control of autonomous vehicles," 2017 American Control Conference (ACC), Seattle, WA, USA, 2017, pp. 4914-4919, doi: 10.23919/ACC.2017.7963716.

[87] Mnih, V., Kavukcuoglu, K., Silver, D. et al. Human-level control through deep reinforcement learning. Nature 518, 529–533, 2015. doi: 10.1038/nature14236

[88] I. Arel, D. C. Rose and T. P. Karnowski, "Deep Machine Learning - A New Frontier in Artificial Intelligence Research [Research Frontier]," in IEEE Computational Intelligence Magazine, vol. 5, no. 4, pp. 13-18, Nov. 2010, doi: 10.1109/MCI.2010.938364.

[89] J. Tani, M. Ito, and Y. Sugita, "Self-organization of distributedly represented multiple behavior schemata in a mirror system: Reviews of robot experiments using RNNPB," Neural Netw., vol. 17, nos. 8–9, pp. 1273–1289, Oct. 2004. doi: 10.1016/j.neunet.2004.05.007

[90] Y. Lecun, Y. Bengio, and G. Hinton, "Deep learning," Nature 521, 436–444, 2015. doi: 10.1038/nature14539

[91] J. Schmidhuber, "Deep learning in neural networks: An overview," Neural networks 61, 2015: 85-117. doi: 10.1016/j.neunet.2014.09.003

[92] M. Zhou, Y. Yu and X. Qu, "Development of an Efficient Driving Strategy for Connected and Automated Vehicles at Signalized Intersections: A Reinforcement Learning Approach," in IEEE Transactions on Intelligent Transportation Systems, vol. 21, no. 1, pp. 433-443, Jan. 2020, doi: 10.1109/TITS.2019.2942014.

[93] Y. Guan et al., "Learn collision-free self-driving skills at urban intersections with model-based reinforcement learning," 2021 IEEE International Intelligent Transportation Systems Conference (ITSC), Indianapolis, IN, USA, 2021, pp. 3462-3469, doi: 10.1109/ITSC48978.2021.9564880.

[94] Shi, Yanjun, et al. "A control method with reinforcement learning for urban un-signalized intersection in hybrid traffic environment." Sensors 22.3, 2022: 779. doi: 10.3390/s22030779

[95] Gutiérrez-Moreno, Rodrigo, et al. "Reinforcement learning-based autonomous driving at intersections in CARLA simulator." Sensors 22.21, 2022: 8373. doi: 10.3390/s22218373

[96] D. Isele, R. Rahimi, A. Cosgun, K. Subramanian and K. Fujimura, "Navigating Occluded Intersections with Autonomous Vehicles Using Deep Reinforcement Learning," 2018 IEEE International Conference on Robotics and Automation (ICRA), Brisbane, QLD, Australia, 2018, pp. 2034-2039, doi: 10.1109/ICRA.2018.8461233.

[97] Li, G., Li, S., Li, S. et al. Deep Reinforcement Learning Enabled Decision-Making for Autonomous Driving at Intersections. Automot. Innov. 3, 374 – 385, 2020. doi: 10.1007/s42154-020-00113-1

[98] H. Shu, T. Liu, X. Mu and D. Cao, "Driving Tasks Transfer Using Deep Reinforcement Learning for Decision-Making of Autonomous Vehicles in Unsignalized Intersection," in IEEE Transactions on Vehicular Technology, vol. 71, no. 1, pp. 41-52, Jan. 2022, doi: 10.1109/TVT.2021.3121985.

[99] D. Kamran, C. F. Lopez, M. Lauer and C. Stiller, "Risk-Aware High-level Decisions for Automated Driving at Occluded Intersections with Reinforcement Learning," 2020 IEEE Intelligent Vehicles Symposium (IV), Las Vegas, NV, USA, 2020, pp. 1205-1212, doi: 10.1109/IV47402.2020.9304606.

[100] T. Tram, I. Batkovic, M. Ali and J. Sjöberg, "Learning When to Drive in Intersections by Combining Reinforcement Learning and Model Predictive Control," 2019 IEEE Intelligent Transportation Systems Conference (ITSC), Auckland, New Zealand, 2019, pp. 3263-3268, doi: 10.1109/ITSC.2019.8916922.

[101] Hausknecht, Matthew, and Peter Stone. "Deep recurrent q-learning for partially observable mdps." 2015 aaai fall symposium series. 2015.

[102] J. Randløv and P. Alstrøm, "Learning to drive a bicycle using reinforcement learning and shaping," in Proc. 15th Int. Conf. Mach. Learn., San Francisco, CA, USA: Morgan Kaufmann, 1998, pp. 463–471.

[103] E. Wiewiora, "Reward shaping," in Encyclopedia of Machine Learning and Data Mining, C. Sammut and G. I. Webb, Eds. Boston, MA, USA: Springer, 2017, pp. 1104–1106.